Received 21 March 2025; revised 30 May 2025; accepted 21 June 2025. Date of publication 1 July 2025; date of current version 1 August 2025.

Digital Object Identifier 10.1109/OJCOMS.2025.3584517

Joint Precoding and Transmit Power Allocation for Multiuser Multiantenna SWIPT Employing OFDM With Optimal Time-Switching and α-Fairness

RICHARD P. KETCHAM (Student Member, IEEE), SOFIE POLLIN (Senior Member, IEEE), AND MARC MOONEN (Fellow, IEEE)

Department of Electrical Engineering (ESAT), KU Leuven, 3001 Leuven, Belgium

CORRESPONDING AUTHOR: R. P. KETCHAM (e-mail: rich.ketcham@gmail.com)

This work was supported in part by the Fonds de la Recherche Scientifique (FNRS) and the Fonds Wetenschappelijk Onderzoek - Vlaanderen through the 'MUlti-SErvice WIreless NEtwork (MUSE-WINET)' under EOS Project 30452698, and in part by the FWO Research through the Project User-centric distributed signal processing algorithms for next generation cell-free massive MIMO based wireless communication networks under Grant G0C0623N.

ABSTRACT Time-switching is a common simultaneous wireless information and power transfer (SWIPT) receiver technique in which the receiver alternates between information decoding and power harvesting, with durations governed by the time-switching ratio. Existing methods for optimizing the time-switching ratio typically rely on convex problem formulations or are restricted to simplified problem structures solvable via the Lambert W function. In multiuser (MU) orthogonal frequency division multiplexing (OFDM) systems, where optimal resource allocation is non-convex due to MU interference, optimizing the time-switching ratio is particularly challenging, as it introduces coupling across subcarriers. Prior work that maximized data rates in MU multiple-input single-output (MISO) OFDM systems – without resorting to interference suppression – did not address time-switching ratio optimization for this reason. This paper presents a method for joint transmit power allocation, precoding, and time-switching ratio optimization in MU-MISO SWIPT systems employing OFDM over the broadcast channel (BC). Rather than treating the time-switching ratio as a fixed parameter, the proposed approach incorporates a recently established mapping between optimal time-switching ratios and weighted resource allocations, enabling efficient per-user optimization. The method is further generalized using α-Fairness utility functions to balance throughput and energy harvesting according to a fairness parameter. By leveraging Lagrange duality and the time-sharing property, the algorithm retains interference as harvestable energy while achieving near-optimal and fair resource allocation.

INDEX TERMS SWIPT, time-switching, energy harvesting, power harvesting, rate-power region, resource allocation, OFDM, precoding, multiuser, multicarrier.

I. INTRODUCTION

THE UTILITY of an energy-constrained wireless network is often limited due to the reliance on finite energy sources. Owing to its potential to assuage this type of constraint, a technology termed simultaneous wireless information and power transfer (SWIPT) has garnered attention. By combining wireless communication and wireless power transfer concepts, SWIPT uses shared resources to deliver power and information simultaneously to remote wireless users thereby alleviating the limitations imposed by the energy constraints. SWIPT related research has covered a wide variety of topics since it was first introduced in [1], [2], [3], but primarily seeks to advance the utilization of limited system resources. Optimal resource allocation is crucial to improving the feasibility of SWIPT, so designing efficient resource allocation methods while incorporating technologies that improve power utilization, such as orthogonal frequency division multiplexing (OFDM) and precoding [4], is essential.

Multiuser (MU) SWIPT's concurrent nature, coupled with the complexity of OFDM and precoding, poses challenging non-convex resource allocation problems. The non-convexity

© 2025 The Authors. This work is licensed under a Creative Commons Attribution 4.0 License.
For more information, see https://creativecommons.org/licenses/by/4.0/

arises, in part, from user interference and normally precludes using Lagrange duality and dual decomposition due to the duality gap, unless the interference is mitigated. The computational complexity of solving the primal problem may be tolerable for a single-carrier system. However, when OFDM is included the computational complexity grows exponentially with the number of subcarriers, making solving the primal problem computationally prohibitive. Hence, when incorporating OFDM, the problem must be decomposable for tractability. While mitigating user interference through orthogonal frequency division multiple access (OFDMA) and zero forcing (ZF) precoding are common ways for enhancing tractability, they are optimal only under high interference conditions [5], [6]. Instead, a novel method for SWIPT presented in [7] exploits hidden convexity within multicarrier systems to enable dual decomposition without resorting to interference mitigation.

In [7], a non-convex optimization problem is first formulated in which a weighted sum of user data rates is maximized subject to meeting total transmit and harvested power constraints for a MU multiple-input single-output (MISO) SWIPT system employing OFDM in the broadcast channel (BC). The time-sharing property of multicarrier systems [8], [9] is observed to justify utilizing Lagrangian duality and dual decomposition despite the non-convexity of the problem formulation. Time-sharing holds that a resource allocation problem has a zero duality gap if a feasible solution can always be constructed by averaging two optimal solutions. This is typically done through scheduling with variable time slots, but multicarrier systems can approximate this by interleaving the achievable resource allocations via the subcarriers [9]. With the time-sharing property, [7] decomposes the problem without resorting to suboptimal interference mitigation methods. This approach then leverages a multiple access channel (MAC)-BC duality to simplify precoder design, linking the problem to the dual MAC transmit power.

In slotted time, a resource allocation is constant for the duration of one or more slots, after which the status of the network is evaluated and a new resource allocation is generated. During each slot, a SWIPT receiver must contend with receiving both information and power. Information decoding and power harvesting are very different operations and the respective receivers have different sensitivities [4]. Due to these fundamental differences, SWIPT receivers are generally modeled as co-located receivers in which the received signal is split between an information decoder and a power harvester [10]. One approach to splitting is to designate each user as an information decoder or power harvester for the duration of the slot. This is known as separated information decoding and power (or energy) harvesting where one or more access points transmit to one or both groups simultaneously [11], [12]. However, compared to signal splitting, this approach reduces system flexibility. Two very common methods used in SWIPT to split the signal are power-splitting and time-switching (or time-splitting). Power-splitting defines a ratio in which a proportion of power is sent to the information decoder and the remaining proportion is used for power harvesting. Time-switching, not to be confused with time-sharing, defines a ratio in which a proportion of the time slot is used for information decoding and the remaining proportion is used for power harvesting.

The power transfer efficiency for SWIPT is very low, making it much more practical for low-power devices like wireless sensors. It is well known that the information decoder is among the most power-consuming components in devices like wireless sensors, so turning it off regularly saves power and extends the device's life [13]. This is a paradigm that naturally suits time-switching. While power-splitting is often preferred because it allows simultaneous information and power transmission, leading to a better trade-off between information rate and energy transfer [10], it has practical limitations compared to time-switching. Time-switching requires only a high-speed RF switch, which is readily available for commercial and industrial applications at low cost [14]. This makes it simple to implement with appropriate switching ratio granularity and range, low power consumption, and space efficiency. In contrast, power-splitting requires greater hardware complexity to support programmable power-splitting ratios with comparable switching granularity and range over adequate bandwidths, and is an ongoing area of research [15], [16]. Implementing power-splitting through low-complexity antenna switching is possible [3], but it requires multiple receiver antennas, enabling only a small set of splitting ratios and generally increases the size of the wireless device. Due to its simplicity, space efficiency, immediate availability at low cost, and applicability to practical SWIPT applications like wireless sensing time-switching is considered here.

Time-switching ratio optimization has been addressed in several SWIPT-related works in which a variety of system formations have been considered. Most works examine optimizing one time-switching ratio for point-to-point relaying [17], [18], [19], [20], [21] or for a single user [22]. Multiple time-switching ratios are considered to a lesser degree. In [23], [24] each user is assigned a time-switching ratio, while each antenna is assigned a time-switching ratio in [25] for single-user multiantenna SWIPT. In optimizing the time-switching ratio, some works can exploit problem convexity and use standard convex optimization tools. In [23], [25], the time-switching ratio is shown to form a perspective function with the objective, which is concave. Energy efficiency optimization is considered in [24], which is convexified through non-linear precoding and the Dinkelbach method. The authors in [21] alternately optimize a single time-switching ratio and precoding vectors with a line search and semidefinite programming, respectively. A suboptimal method is also presented that uses the Lambert W function to solve problems in the form of $z = xe^x$ for x. Other works that utilize the Lambert W function include [17], [18], [19], [20]. A different approach has been presented in [26], which examines the geometrical relationship between optimal

time-switching ratios in a MU system and the solution to a SWIPT resource allocation problem framed as a weighted sum optimization. It has been shown that a simple, yet novel, relationship exists between the solution to the resource allocation and the optimal time-switching ratios.

The study in [7] overlooks several aspects of resource allocation for SWIPT. Firstly, the method presented failed to optimize the time-switching ratios, instead treating them as fixed parameters. This is in part due to the coupling of the subcarriers through the time-switching ratios, which would have prevented the use of Lagrangian decomposition. Moreover, it disregarded scenarios where specific harvesting constraints remain unknown. Take, for instance, the open systems interconnection (OSI) model, which abstracts various responsibilities and information within a computing system into distinct layers, such as relegating resource allocation to the data link layer. Rather than directly conveying specific harvesting constraints to the data link layer for resource allocation, an upper layer may transmit a weight reflecting not only power and data requirements but also other quality of service (QoS) metrics. Furthermore, ensuring equitable user QoS (i.e., fairness) is a common consideration. One approach to achieving fairness among users is by utilizing a parameterized class of utility functions collectively referred to as α-Fairness [27]. These utility functions allow for the specification of a relative degree of fairness, ranging from utilitarian fairness, which maximizes total throughput, to maximizing the minimum amount of fairness.

In this paper, we seek to combine the results from both [7] and [26] into an efficient near-optimal resource allocation method that jointly allocates power, designs precoding vectors, and chooses per-user time-switching ratios for a MU-MISO-BC SWIPT system employing OFDM. We consider a use case that incorporates fairness and does not support specific harvesting constraints. The objective for the resource allocation problem is first generalized from a weighted sum of data rates to a weighted sum of data rates and harvested powers individually encapsulated in α-Fairness utility functions. Equations for the optimal time-switching ratios as a function of the fairness parameter are derived for the α-fair objective. To support this use case, the resource allocation problem presented in [7] is reformulated as a weighted sum of data rates and harvested powers, which is then used to iteratively solve the resource allocation problem with the α-fair objective using optimal time-switching ratios derived from the mapping presented in [26]. The resulting formulation led to new insights into the relationship between the time-switching ratio, the system weights, and the fairness parameter, which resulted in a near-optimal relative resource allocation method that incorporates varying levels of fairness.

The contributions of this paper include:

- Extending the work in [7] by generalizing from a weighted sum of data rates with total transmit power and power harvesting constraints to a weighted sum of data rates and harvested powers individually encapsulated in α-Fairness utility functions. This has two consequences, first the resource allocation is now relative since there are no power harvesting constraints. Second, generalized fairness between user objectives is now incorporated.
- Extending the mapping for the optimal time-switching ratio developed in [26] for a weighted sum of data rates and harvested powers by generalizing to a weighted sum of data rates and harvested powers encapsulated in α-Fairness utility functions. An equation is derived that maps the weights and α-fair resource allocation to the optimal time-switching ratio.
- Providing an algorithm to optimize multiple time-switching ratios for MU-MISO-SWIPT employing OFDM in the BC.
- Lastly, this paper develops insight into special cases with α-fair resource allocation. In particular, a closed form solution for the optimal time-switching ratio given the weights is provided for log-fair (i.e., proportional fairness) resource allocations.

A. ORGANIZATION

The system model is described in Section II. The results from [26] on optimal time-switching are reviewed in Section III. In Section IV, the problem formulations reviewed in Section III are generalized by using α-fair objectives and the formulas for the optimal time-switching ratios are subsequently derived. In Section V, the resource allocation from [7] is converted to a weighted sum of data rates and harvested powers, which is used to iteratively maximize the linearized α-fair problem formulations presented in Section IV. A formulation is given for the optimal time-switching ratios as a function of the fairness parameter. The algorithms are presented in Section VI and the simulation results are illustrated in Section VII.

B. NOTATION

Matrices are upright and sans-serif, vectors are italicized and bold, and scalars are italicized. Sets are upright, serif, and italicized. The transpose operation is denoted with $(\cdot)^\top$, $(\cdot)^{\mathcal{H}}$ is the Hermitian transpose operation, and $\mathbb{E}[\cdot]$ is the expected value operator. The $diag(\cdot)$ operator returns a diagonal matrix with the diagonal elements given by its argument. The $[\cdot]_{j,i}$ operator refers to the (j, i)-th element of a matrix, where j refers to the row number and i is the column number. "Big O" notation, denoted with $O(\cdot)$, defines the asymptotic upper bound. A set is denoted with $\{\cdot_i\}_{\forall i}$, where i is an index and $\cdot_i$ is the i-th object in the set. The Hadamard product is denoted with $\circ$ and Hadamard division is denoted with $\oslash$. The modulus operation is denoted with $|\cdot|$.

The following variable conventions are used in the manuscript. A harvested power is denoted with a p and a data rate is denoted with a d. The objectives (i.e., harvested power or data rate) are denoted with r. Weights used with a linear utility function are denoted with w while weights used

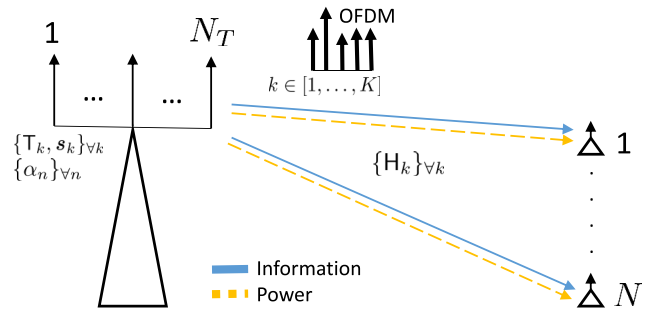

FIGURE 1. OFDM-based MU-MISO-BC-SWIPT system diagram.

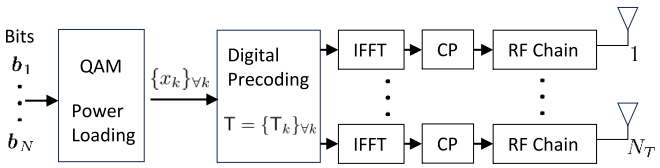

FIGURE 2. A block diagram of a multiantenna OFDM transmitter. Note that $b_1 \ldots b_N$ represent the bit-vectors for users 1 through N, IFFT is the inverse FFT, and CP denotes the addition of the cyclic prefix. The RF Chain block refers to the digital-to-analog converter, filtering, power amplifier, and upconversion to the carrier frequency.

with the α-Fairness utility functions are denoted with μ. Time-switched variables are denoted with the hat symbol $\hat{\cdot}$.

II. SYSTEM MODEL

A SWIPT network is considered that contains one access point and N remote devices (users), each with one antenna. Wireless transmissions are modeled as a BC in which the access point uses N_T transmit antennas to deliver data and power to the N users, where $N \leq N_T$. The network employs OFDM, where the OFDM symbols are comprised of K orthogonal subcarriers. It is assumed that perfect channel state information (CSI) is available and each subcarrier may be modeled independently due to the absence of inter-carrier interference. This assumption is justified by the use of a cyclic prefix of sufficient length, which prevents intersymbol interference (ISI) and maintains the orthogonality of subcarriers. Fig. 1 illustrates the SWIPT network.

A. BROADCAST CHANNEL

The access point applies a precoder to the symbol vector before transmitting to the users, which is modeled on each subcarrier (denoted with subscript k) as a BC with

$$\boldsymbol{y}_k = \mathsf{H}_k^{\mathcal{H}} \mathsf{T}_k \boldsymbol{x}_k + \boldsymbol{z}_k. \tag{1}$$

In (1), $\mathsf{H}_k^{\mathcal{H}}$ is the $N \times N_{\mathrm{T}}$ complex channel matrix, with $[\mathsf{H}_k]_{m,n}^{\mathcal{H}}$ being the transfer function between transmit antenna m and user n evaluated at subcarrier k. The noise variables $\boldsymbol{z}_k$ is an $N \times 1$ complex vector of circularly symmetric additive white Gaussian noise (AWGN) where the distribution of the n-th element is denoted as $z_{k,n} \sim \mathcal{CN}(0, \sigma_{k,n})$ with zero mean and variance $\sigma_{k,n}$. Moreover, $\boldsymbol{x}_k$ is the $N \times 1$ complex vector of transmit symbols for the N users, T_k is the $N_T \times N$ linear complex precoder matrix, and $\boldsymbol{y}_k$ is the $N \times 1$ complex vector of symbols as received by the N users. Fig. 2 illustrates the signal flow through the multiantenna OFDM transmitter.

B. METRICS

The data rate for user n on subcarrier k is modeled with

$$R_{k,n}(\mathsf{T}_k, \boldsymbol{s}_k) = \log_2\Big(1 + \gamma_{k,n}^{\mathrm{BC}}(\mathsf{T}_k, \boldsymbol{s}_k)\Big) \tag{2}$$

and the total data rate for user n is found by summing (2) over all subcarriers. The signal-to-interference-plus-noise ratio (SINR) for user n on subcarrier k, $\gamma_{k,n}^{\mathrm{BC}}(\mathsf{T}_k, \boldsymbol{s}_k)$, is a function of the precoder matrix T_k and symbol power vector $\boldsymbol{s}_k$. The n-th element of $\boldsymbol{s}_k$, denoted by $s_{k,n}$, is the non-negative real-valued symbol power for user n. It is defined as $s_{k,n} \triangleq \mathbb{E}[|x_{k,n}|^2]$, where $x_{k,n}$ is the n-th element of $\boldsymbol{x}_k$ and $\mathbb{E}[\,\cdot\,]$ is the expected value operator. The SINR is given by

$$\gamma_{k,n}^{\mathrm{BC}}(\mathsf{T}_k, \boldsymbol{s}_k) = \frac{|\boldsymbol{t}_{k,n}^{\mathcal{H}} \boldsymbol{h}_{k,n}|^2 s_{k,n}}{\sum_{\substack{m=1 \\ m \neq n}}^{N} |\boldsymbol{t}_{k,m}^{\mathcal{H}} \boldsymbol{h}_{k,n}|^2 s_{k,m} + \sigma_{k,n}}, \tag{3}$$

where $\boldsymbol{t}_{k,n}$ is the $N_T \times 1$ complex precoder vector for user n, i.e., the n-th column of T_k, and $\boldsymbol{h}_{k,n}$ is the $N_T \times 1$ complex channel vector from the access point to user n, i.e., the n-th column of H_k. The additive white Gaussian noise power spectral density experienced by user n on subcarrier k is given by $\sigma_{k,n}$. In this paper, setting T_k and $\boldsymbol{s}_k$ for all subcarriers is referred to as a resource allocation.

It has been observed that the energy harvesting operation is non-linear due to the rectifying circuitry entering saturation, however, this effect may be mitigated by placing several energy harvesting circuits in parallel to enlarge the linear power conversion region [28], [29]. As such, this paper will focus on deriving a resource allocation algorithm without addressing the impact of the power harvesting non-linearity. The received power for user n on subcarrier k is therefore modeled with

$$P_{k,n}(\mathsf{T}_k, \boldsymbol{s}_k) = \sum_{m=1}^{N} |\boldsymbol{t}_{k,m}^{\mathcal{H}} \boldsymbol{h}_{k,n}|^2 s_{k,m} \tag{4}$$

and the total received power for user n is found by summing (4) over all subcarriers (see formula (8)). The efficiency of the power harvesting operation is considered constant, so will not be considered in this work without loss of generality (w.l.o.g).

The total transmit power for user n may be calculated by summing the transmit power over all subcarriers and may be modeled with

$$p_n = \sum_{k=1}^{K} s_{k,n} ||\boldsymbol{t}_{k,n}||_2^2. \tag{5}$$

C. TIME-SWITCHING RECEIVER

The time-switching receiver architecture is incorporated through the time-switching ratio, given by $\alpha_n \in [0, 1]$ for each user n. The receiver for user n spends α_n proportion of time decoding information and $1 - \alpha_n$ harvesting power. Defining

$$r_{d_n} = \sum_{k=1}^{K} R_{k,n}(\mathsf{T}_k, \boldsymbol{s}_k), \tag{6}$$

the achieved average data rate is then given by

$$\hat{r}_{d_n} = \alpha_n r_{d_n}, \tag{7}$$

where $\hat{r}_{d_n}$ is the resulting data rate for user n due to time-switching. Similarly, defining

$$r_{p_n} = \sum_{k=1}^{K} P_{k,n}(\mathsf{T}_k, \boldsymbol{s}_k), \tag{8}$$

the achieved average harvested power is given by

$$\hat{r}_{p_n} = (1 - \alpha_n) r_{p_n}, \tag{9}$$

where $\hat{r}_{p_n}$ is the resulting harvested power for user n due to time-switching. It is clear from (7) and (9) that there is an inverse relationship between the data rate and the harvested power for each user due to the time-switching ratio. The maximum data rate for user n occurs when $\alpha_n = 1$. Similarly, the maximum harvested power for user n occurs when $\alpha_n = 0$.

Note that the p and d midscripts denote the power and data rate, respectively. Lastly, the set $\{r_{p_n}, r_{d_n}\}_{\forall n}$ denotes all data rate r_{d_n} and harvested power r_{p_n} pairs for each user n. Likewise, the set $\{\hat{r}_{p_n}, \hat{r}_{d_n}\}_{\forall n}$ denotes all time-switched data rate $\hat{r}_{d_n}$ and harvested power $\hat{r}_{p_n}$ pairs for each user n.

III. RATE-POWER REGIONS AND TIME-SWITCHING

A rate-power region (RPR) characterizes the set of all achievable data rates and harvested powers for a given SWIPT transmit resource allocation problem. It captures the fundamental trade-off between data rate and power harvesting. For a given wireless channel, each point in the region corresponds to a feasible allocation of transmit resources (i.e., precoding vectors, power allocation, and time-switching ratio parameters). The boundary of the RPR represents the Pareto-optimal trade-off, where improving one objective requires sacrificing the other. Three distinct RPRs — the Fixed-$\boldsymbol{\alpha}$ RPR, the Utopia RPR, and the Optimal RPR — and how they relate through the time-switching ratio were described in [26]. For clarity, these regions are briefly defined in Section III-A, and illustrated for a single-user scenario in Fig. 3.

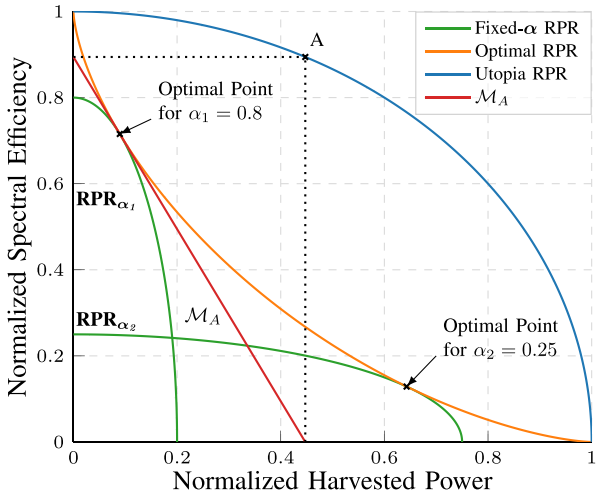

FIGURE 3. Depiction of the Utopia RPR, the Optimal RPR, and two Fixed-α RPRs for a single user. A Utopia point is the non-time-switched point $\{r_p, r_d\}$ resulting from (P1) for a given set of weights $\{w_p, w_d\}$. The collection of all Utopia points defines the Utopia RPR. A Fixed-α RPR results when the Utopia RPR is time-switched with a fixed time-switching ratio (e.g. α_1 or α_2 in the figure). A time-switched point is denoted with $\{\hat{r}_p, \hat{r}_d\}$ and results from (P1). Time-switching each point on the Pareto edge of the Utopia RPR with the associated optimal time-switching ratio results in the Pareto edge of the Optimal RPR. A particular fixed time-switching ratio is optimal at the point the associated Fixed-α RPR intersects the Optimal RPR. The rate-power manifold $\mathcal{M}_A$ is generated when Utopia point A is time-switched by all possible time-switching ratio values.

A. RATE-POWER REGION DEFINITIONS

From a time-switching perspective, the non-time-switched point $\{r_{p_n}, r_{d_n}\}_{\forall n}$ as defined in (6) and (8) is mostly unobtainable, as it would require the time-switching ratio to be 0 and 1 simultaneously, so it is referred to as a Utopia point. The collection of Utopia points defines the Utopia RPR. If time-switching is applied, denoted with $\{\hat{r}_{p_n}, \hat{r}_{d_n}\}_{\forall n}$ in (7) and (9), then the Utopia RPR is scaled by the time-switching ratio and the resulting region is referred to as the Fixed-$\boldsymbol{\alpha}$ RPR and denoted with $RPR_{\boldsymbol{\alpha}}$ for $\boldsymbol{\alpha} = [\alpha_1, \ldots, \alpha_N]^\top$. The union of all Fixed-$\boldsymbol{\alpha}$ RPRs for all possible time-switching ratios is referred to as the Optimal RPR. Fixed-$\boldsymbol{\alpha}$ RPRs will intersect the Pareto edge of the Optimal RPR at the points where the particular set of time-switching ratios is optimal, as shown for a single user in Fig. 3. By fixing $\boldsymbol{\alpha}$, the Fixed-$\boldsymbol{\alpha}$ RPR is strictly dominated by the Optimal RPR. While it may contain feasible points, optimality cannot be guaranteed for the specific resource allocation problem as $\boldsymbol{\alpha}$ is fixed. However, there will always be a resource allocation problem with an associated set of harvested power constraints for which the fixed $\boldsymbol{\alpha}$ is optimal and this set of harvested power constraints is given by the intersection of the Fixed-$\boldsymbol{\alpha}$ RPR and the Optimal RPR. Lastly, an N-dimensional rate-power manifold $\mathcal{M}$ (e.g. $\mathcal{M}_A$ in Fig. 3) is produced when a particular Utopia point (point A in Fig. 3, for example) is time-switched with all possible values of the time-switching ratios.

B. RATE-POWER REGION PROBLEM FORMULATION

Points on the Utopia RPR are found by maximizing a weighted sum of data rates and harvested powers without

time-switching

$$\begin{aligned} \underset{\mathsf{T},\mathsf{s}}{\text{maximize}} \quad & \sum_{n=1}^{N} w_{d_n} r_{d_n} + w_{p_n} r_{p_n} \\ \text{s.t.} \quad & \sum_{n=1}^{N} p_n \leq P_{\text{Total}} \\ & s_{k,n} \geq 0 \quad \forall\, k, n, \end{aligned} \tag{P1}$$

where $\mathsf{T} = \{\mathsf{T}_k\}_{\forall k}$, $\mathsf{s} = \{\boldsymbol{s}_k\}_{\forall k}$, and the total transmit power is constrained to P_{Total}. The non-negative real-valued weights w_{d_n} and w_{p_n} are used to weight the user data rates and harvested powers. The weights define a hyperplane that is tangent to Utopia RPR. The point of tangency is known as a Utopia point and is the solution to (P1) for the given weights. The Pareto edge of the Utopia RPR is presumed to be concave due to the time-sharing property (see Section V-D) and can thus be traced by varying these weights [30].

Similarly, points on a Fixed-$\boldsymbol{\alpha}$ RPR are found by maximizing a weighted sum of time-switched data rates and harvested powers for a fixed set of time-switching ratios $\boldsymbol{\alpha}$

$$\begin{aligned} \underset{\mathsf{T},\mathsf{s}}{\text{maximize}} \quad & \sum_{n=1}^{N} \hat{w}_{d_n} \hat{r}_{d_n} + \hat{w}_{p_n} \hat{r}_{p_n} \\ \text{s.t.} \quad & \sum_{n=1}^{N} p_n \leq P_{\text{Total}} \\ & s_{k,n} \geq 0 \quad \forall\, k, n. \end{aligned} \tag{$\overline{\text{P1}}$}$$

The time-switched weights $\hat{w}_{d_n}$ and $\hat{w}_{p_n}$ are used to weight the user data rate and harvested power, respectively, and take on non-negative real values. They define a hyperplane that is tangent to the solution of ($\overline{\text{P1}}$). The Pareto edge of the particular Fixed-$\boldsymbol{\alpha}$ RPR is presumed to be concave due to the time-sharing property and can thus be traced by varying these weights (see Section V-D).

To find a point on the Optimal RPR the time-switching ratio may be included as an optimization parameter leading to

$$\begin{aligned} \underset{\mathsf{T},\mathsf{s},\boldsymbol{\alpha}}{\text{maximize}} \quad & \sum_{n=1}^{N} \hat{w}_{d_n} \hat{r}_{d_n} + \hat{w}_{p_n} \hat{r}_{p_n} \\ \text{s.t.} \quad & \sum_{n=1}^{N} p_n \leq P_{\text{Total}} \\ & \alpha_n \in [0, 1] \quad \forall\, n \\ & s_{k,n} \geq 0 \quad \forall\, k, n. \end{aligned} \tag{$\widehat{\text{P1}}$}$$

The time-switched weights define a hyperplane tangent to the solution of ($\widehat{\text{P1}}$). However, due to the non-concavity of the Optimal RPR, solutions to ($\widehat{\text{P1}}$) will only correspond to the corner points of the Optimal RPR. More generally, a point is on the Optimal RPR when the hyperplane defined by the time-switched weights is simultaneously tangent to both the Fixed-$\boldsymbol{\alpha}$ RPR and the Optimal RPR at the same time-switched point [26]. To address this issue, in Section IV, ($\widehat{\text{P1}}$) will be modified into ($\widehat{\text{P2}}$).

C. INFLUENCE OF THE TIME-SWITCHING RATIO

Problems (P1) and ($\overline{\text{P1}}$) will choose the same resource allocation T s if for each user n [26]

$$w_{p_n} r_{p_n} = \hat{w}_{p_n} \hat{r}_{p_n} \tag{10}$$

and

$$w_{d_n} r_{d_n} = \hat{w}_{d_n} \hat{r}_{d_n}, \tag{11}$$

meaning that solving ($\overline{\text{P1}}$) for a fixed set of time-switching ratios corresponds to solving (P1) with weights

$$\left\{w_{p_n}, w_{d_n}\right\}_{\forall n} = \left\{\hat{w}_{p_n}(1-\alpha_n), \hat{w}_{d_n}\alpha_n\right\}_{\forall\, n} \tag{12}$$

with corresponding solutions

$$\left\{r_{p_n}, r_{d_n}\right\}_{\forall n} = \left\{\frac{\hat{r}_{p_n}}{(1-\alpha_n)}, \frac{\hat{r}_{d_n}}{\alpha_n}\right\}_{\forall\, n}. \tag{13}$$

In other words, a solution to ($\overline{\text{P1}}$) also defines a Utopia point $\left\{r_{p_n}, r_{d_n}\right\}_{\forall n}$ through (13), which is the solution to (P1) with weights defined through (12).

D. OPTIMAL TIME-SWITCHING RATIO

If a set of time-switching ratios is used to time-switch a particular Utopia point $\left\{r_{p_n}, r_{d_n}\right\}_{\forall n}$ and results in a time-switched point $\left\{\hat{r}_{p_n}, \hat{r}_{d_n}\right\}_{\forall n}$ that lies on the Pareto edge of the Optimal RPR, then the time-switching ratios are considered optimal for that particular Utopia point and are denoted with $\boldsymbol{\alpha}^*$. In [26], a mapping was developed for user n that relates the associated weights and resulting resource allocation found through (P1) and ($\overline{\text{P1}}$) to the optimal time-switching ratio for user n, α_n^*. For a resource allocation found through (P1), the optimal time-switching ratio with respect to (w.r.t.) the resource allocation for user n is given by Lemma 1. Similarly, for a resource allocation found through ($\overline{\text{P1}}$) the optimal time-switching ratio w.r.t. the resource allocation for user n is given by Lemma 2.

Lemma 1 (Propositions 1 and 2 From [26]): The optimal time-switching ratio for the non-time-switched resource allocation corresponding to $\left\{r_{p_n}, r_{d_n}\right\}_{\forall n}$ that is optimal in (P1) for weights $\left\{w_{p_n}, w_{d_n}\right\}_{\forall n}$ is simultaneously given by

$$\alpha_n^* = \frac{w_{d_n} r_{d_n}}{w_{p_n} r_{p_n} + w_{d_n} r_{d_n}} \tag{14}$$

and

$$1 - \alpha_n^* = \frac{w_{p_n} r_{p_n}}{w_{p_n} r_{p_n} + w_{d_n} r_{d_n}}. \tag{15}$$

Proof: Please refer to [26] for details. ■

Lemma 2: The optimal time-switching ratio for the time-switched resource allocation corresponding to $\left\{\hat{r}_{p_n}, \hat{r}_{d_n}\right\}_{\forall n}$

that is optimal in (P̄1) for weights $\{\hat{w}_{p_n}, \hat{w}_{d_n}\}_{\forall n}$ is simultaneously given by

$$\alpha_n^* = \frac{\hat{w}_{d_n}\hat{r}_{d_n}}{\hat{w}_{d_n}\hat{r}_{d_n} + \hat{w}_{p_n}\hat{r}_{p_n}} \tag{16}$$

and

$$1 - \alpha_n^* = \frac{\hat{w}_{p_n}\hat{r}_{p_n}}{\hat{w}_{d_n}\hat{r}_{d_n} + \hat{w}_{p_n}\hat{r}_{p_n}}. \tag{17}$$

Proof: Choosing a set of weights $\{\hat{w}_{p_n}, \hat{w}_{d_n}\}_{\forall n}$ and time-switching ratios $\boldsymbol{\alpha}$, solving (P̄1) results in the time-switched resource allocation $\{\hat{r}_{p_n}, \hat{r}_{d_n}\}_{\forall n}$. Equations (12) and (13) describe the relationship between the time-switched and non-time-switched weights and resource allocations. Substituting (12) and (13) into (14) and (15) expresses the optimal time-switching ratio formulas in terms of the time-switched weights and resource allocations, leading to (16) and (17), respectively. ■

IV. α-FAIRNESS AND TIME-SWITCHING

In this section the formulations introduced in Section III are generalized by incorporating fairness between the user objectives via a parameterized set of utility functions collectively termed α-Fairness, which was proposed in [27]. These utility functions exhibit increasing non-linearity w.r.t. the fairness parameter, making individual objective functions more responsive to subtle variations and consequently improving QoS fairness. Furthermore, non-linear utility functions, such as α-fair utility functions, define curved hypersurfaces. As the curvature of these hypersurfaces increases, they become increasingly capable of finding solutions within non-convex regions of the Pareto surface [31]. Thus, this generalization offers the added advantage of enhancing the optimization's efficacy in capturing Pareto optimal points.

A. α-FAIRNESS

The utility functions defined by α-Fairness utilize a parameter that is usually denoted with α but will be denoted with β herein to avoid confusion with the time-switching ratio. The utility functions are then defined as

$$f^{\beta}(\{z_n\}_{\forall n}) = \begin{cases} \sum_{n=1}^{N} \mu_n \frac{(z_n)^{1-\beta}}{(1-\beta)}, & \beta \geq 0, \beta \neq 1 \\ \sum_{n=1}^{N} \mu_n \ln(z_n), & \beta = 1, \end{cases} \tag{18}$$

where $\{z_n\}_{\forall n}$ represents the set of objectives, μ_n is a weight associated with the n-th objective, and β is the fairness parameter [27]. As the fairness parameter β increases, the utility functions encourage increasingly equivalent objectives thereby increasing fairness. Note that the natural logarithm is used for $\beta = 1$ and when $\beta = 0$, (18) reduces to the linear utility function like that examined in Section III. Lastly, if the objectives differ in type (e.g. data rate vs. harvested power), it becomes paramount to appropriately scale the objectives by their possible range of values, otherwise, a particular objective may be promoted more than it should. It is assumed that the objectives are appropriately scaled.

B. α-FAIR PROBLEM FORMULATION

In this application, the set of objectives includes data rates and harvested powers, so

$$\{z_n\}_{\forall n} = \begin{cases} \{r_{p_n}, r_{d_n}\}_{\forall n}, & \text{if not time-switched} \\ \{\hat{r}_{p_n}, \hat{r}_{d_n}\}_{\forall n}, & \text{if time-switched.} \end{cases} \tag{19}$$

Likewise, the weights are denoted with $\{\mu_{p_n}, \mu_{d_n}\}_{\forall n}$ if not time-switched or $\{\hat{\mu}_{p_n}, \hat{\mu}_{d_n}\}_{\forall n}$ if time-switched. The objective functions are then

$$\begin{aligned} &\beta \neq 1 \ , \beta \geq 0\text{:} \\ &\qquad f^{\beta} = \sum_{n=1}^{N} \left(\frac{\mu_{p_n}}{(r_{p_n})^{\beta-1}} + \frac{\mu_{d_n}}{(r_{d_n})^{\beta-1}} \right) (1-\beta)^{-1} \\ &\beta = 1 \ : \\ &\qquad f^{\beta} = \sum_{n=1}^{N} \mu_{p_n} \ln(r_{p_n}) + \mu_{d_n} \ln(r_{d_n}) \end{aligned} \tag{20}$$

or

$$\begin{aligned} &\beta \neq 1 \ , \beta \geq 0\text{:} \\ &\qquad \hat{f}^{\beta} = \sum_{n=1}^{N} \left(\frac{\hat{\mu}_{p_n}}{(\hat{r}_{p_n})^{\beta-1}} + \frac{\hat{\mu}_{d_n}}{(\hat{r}_{d_n})^{\beta-1}} \right) (1-\beta)^{-1} \\ &\beta = 1 \ : \\ &\qquad \hat{f}^{\beta} = \sum_{n=1}^{N} \hat{\mu}_{p_n} \ln(\hat{r}_{p_n}) + \hat{\mu}_{d_n} \ln(\hat{r}_{d_n}) \end{aligned} \tag{21}$$

if time-switched. Problem (P1) can then be generalized as

$$\begin{aligned} \underset{\mathsf{T},\mathsf{s}}{\text{maximize}} \quad & f^{\beta} \\ \text{s.t.} \quad & \sum_{n=1}^{N} p_n \leq P_{\text{Total}} \\ & s_{k,n} \geq 0 \quad \forall\, k, n, \end{aligned} \tag{P2}$$

(P̄1) can be generalized as

$$\begin{aligned} \underset{\mathsf{T},\mathsf{s}}{\text{maximize}} \quad & \hat{f}^{\beta} \\ \text{s.t.} \quad & \sum_{n=1}^{N} p_n \leq P_{\text{Total}} \\ & s_{k,n} \geq 0 \quad \forall\, k, n, \end{aligned} \tag{P̄2}$$

and (P̂1) can be generalized as

$$\begin{aligned} \underset{\mathsf{T},\mathsf{s},\boldsymbol{\alpha}}{\text{maximize}} \quad & \hat{f}^{\beta} \\ \text{s.t.} \quad & \sum_{n=1}^{N} p_n \leq P_{\text{Total}} \\ & \alpha_n \in [0,1] \quad \forall\, n \\ & s_{k,n} \geq 0 \quad \forall\, k, n. \end{aligned} \tag{P̂2}$$

Note that if $\alpha_n \in \{0, 1\}$, either the harvested power objective or the data rate objective for user n will need to be removed from the optimization for $\beta \geq 1$ because it will be unbounded otherwise. $\hat{f}^{\beta}$ is bounded for time-switching ratios on $[a, b]$ provided that $0 < a < b < 1$ and if we set $\hat{\mu}_{p_n} = 0$ when $\alpha_n > b$ and $\hat{\mu}_{d_n} = 0$ when $\alpha_n < a$ for all users n.

C. α-FAIRNESS AND OPTIMAL TIME-SWITCHING

Expressions for the optimal time-switching ratio are developed for points found on the Fixed-$\boldsymbol{\alpha}$ RPR in Proposition 1 using (P2) and for points found on the Utopia RPR in Proposition 2 using (P2). Note that the total transmit power constraint does not involve the objectives so the discussion will exclusively focus on the objective function for the rest of Section IV.

Proposition 1: The optimal time-switching ratio for the time-switched resource allocation corresponding to $\{\hat{r}_{p_n}, \hat{r}_{d_n}\}_{\forall n}$ that is optimal in (P2) for weights $\{\hat{\mu}_{p_n}, \hat{\mu}_{d_n}\}_{\forall n}$ is simultaneously given by

$$\alpha_n^* = \frac{\hat{\mu}_{d_n}}{\left(\hat{r}_{d_n}\right)^{\beta-1}}\left(\frac{\hat{\mu}_{p_n}}{\left(\hat{r}_{p_n}\right)^{\beta-1}} + \frac{\hat{\mu}_{d_n}}{\left(\hat{r}_{d_n}\right)^{\beta-1}}\right)^{-1} \tag{22}$$

and

$$1 - \alpha_n^* = \frac{\hat{\mu}_{p_n}}{\left(\hat{r}_{p_n}\right)^{\beta-1}}\left(\frac{\hat{\mu}_{p_n}}{\left(\hat{r}_{p_n}\right)^{\beta-1}} + \frac{\hat{\mu}_{d_n}}{\left(\hat{r}_{d_n}\right)^{\beta-1}}\right)^{-1}. \tag{23}$$

Proof: If (P2) and (P1) result in the same point on the Fixed-$\boldsymbol{\alpha}$ RPR, then they have the same tangents that are given by

$$\nabla \hat{f}^{\beta} = \left[\frac{\hat{\mu}_{p_n}}{\left(\hat{r}_{p_n}\right)^{\beta}}, \frac{\hat{\mu}_{d_n}}{\left(\hat{r}_{d_n}\right)^{\beta}}\right]_{\forall n}^{\top} \tag{24}$$

and

$$\nabla \hat{f}^{\mathrm{WS}} = \left[\hat{w}_{p_n}, \hat{w}_{d_n}\right]_{\forall n}^{\top}, \tag{25}$$

where $\hat{f}^{\mathrm{WS}}$ denotes the objective of (P1). Setting (24) equal to (25) such that

$$\left[\hat{w}_{p_n} = \frac{\hat{\mu}_{p_n}}{\left(\hat{r}_{p_n}\right)^{\beta}}, \hat{w}_{d_n} = \frac{\hat{\mu}_{d_n}}{\left(\hat{r}_{d_n}\right)^{\beta}}\right]_{\forall n}^{\top}, \tag{26}$$

and substituting the coefficients into (16) yields

$$\begin{aligned}\alpha_n^* &= \frac{\hat{w}_{d_n}\hat{r}_{d_n}}{\hat{w}_{p_n}\hat{r}_{p_n} + \hat{w}_{d_n}\hat{r}_{d_n}} \\ &= \frac{\hat{\mu}_{d_n}}{\left(\hat{r}_{d_n}\right)^{\beta-1}}\left(\frac{\hat{\mu}_{p_n}}{\left(\hat{r}_{p_n}\right)^{\beta-1}} + \frac{\hat{\mu}_{d_n}}{\left(\hat{r}_{d_n}\right)^{\beta-1}}\right)^{-1}\end{aligned} \tag{27}$$

for all users n. Substituting the coefficients into (17) similarly finds that $(1 - \alpha_n^*)$ is the same as (23) and thus proves the proposition. ■

Proposition 2: The optimal time-switching ratio for the non-time-switched resource allocation corresponding to $\{r_{p_n}, r_{d_n}\}_{\forall n}$ that is optimal in (P2) for weights $\{\mu_{p_n}, \mu_{d_n}\}_{\forall n}$ is simultaneously given by

$$\alpha_n^* = \frac{\mu_{d_n}}{\left(r_{d_n}\right)^{\beta-1}}\left(\frac{\mu_{p_n}}{\left(r_{p_n}\right)^{\beta-1}} + \frac{\mu_{d_n}}{\left(r_{d_n}\right)^{\beta-1}}\right)^{-1} \tag{28}$$

and

$$1 - \alpha_n^* = \frac{\mu_{p_n}}{\left(r_{p_n}\right)^{\beta-1}}\left(\frac{\mu_{p_n}}{\left(r_{p_n}\right)^{\beta-1}} + \frac{\mu_{d_n}}{\left(r_{d_n}\right)^{\beta-1}}\right)^{-1}. \tag{29}$$

Proof: The proof is similar to that for Proposition 1 if applied to the Utopia RPR instead of a Fixed-$\boldsymbol{\alpha}$ RPR. If (P1) and (P2) result in the same point on the Utopia RPR, then they have the same tangents that are given by

$$\nabla f^{\mathrm{WS}} = \left[w_{p_n}, w_{d_n}\right]_{\forall n}^{\top}, \tag{30}$$

and

$$\nabla f^{\beta} = \left[\frac{\mu_{p_n}}{\left(r_{p_n}\right)^{\beta}}, \frac{\mu_{d_n}}{\left(r_{d_n}\right)^{\beta}}\right]_{\forall n}^{\top} \tag{31}$$

where f^{WS} denotes the objective of (P1). Setting (31) equal to (30) such that

$$\left[w_{p_n} = \frac{\mu_{p_n}}{\left(r_{p_n}\right)^{\beta}}, w_{d_n} = \frac{\mu_{d_n}}{\left(r_{d_n}\right)^{\beta}}\right]_{\forall n}^{\top}, \tag{32}$$

and substituting the coefficients into (14) yields

$$\begin{aligned}\alpha_n^* &= \frac{w_{d_n} r_{d_n}}{w_{p_n} r_{p_n} + w_{d_n} r_{d_n}} \\ &= \frac{\mu_{d_n}}{\left(r_{d_n}\right)^{\beta-1}}\left(\frac{\mu_{p_n}}{\left(r_{p_n}\right)^{\beta-1}} + \frac{\mu_{d_n}}{\left(r_{d_n}\right)^{\beta-1}}\right)^{-1}\end{aligned} \tag{33}$$

for all users n. Substituting the coefficients into (15) similarly finds that $(1 - \alpha_n^*)$ is the same as (29) and thus proves the proposition. ■

V. JOINT α-FAIR RESOURCE ALLOCATION AND TIME-SWITCHING OPTIMIZATION

As noted in Section I, there are situations when the harvesting constraints are unknown, so the formulation examined in [7] may not be applicable. For example, an upper layer in the OSI model may send weights that reflect not only the power and data requirements but also other QoS metrics like fairness. Instead, this section will employ the methods developed in [7] to solve the generalized problem developed in Section IV, which allocates resources relatively based on the weights assigned to the individual objectives and the fairness parameter. Expressions and methods for determining the optimal resource allocation including the optimal time-switching ratio will then be developed.

The primal problem is given in (P2). It is a challenging non-convex problem, which cannot be directly solved using the methods developed in [7] because the time-switching ratios couple the subcarriers. Instead, (P2) will be solved through the so-called alternating optimization (AO) approach where (P2) is solved for each iterate of the time-switching ratios and the time-switching ratios are adjusted in the ascent direction until the iterates converge to the optimal value. Additionally, the non-linear utility functions in (P2) also complicate directly utilizing the methods developed in [7]. Instead, (P2) will be solved by iteratively maximizing a linearized version of it, which is in the same form as (P1). This section will first review the methods developed in [7] by applying them to solve (P1). The discussion will then motivate the rest of the solution method.

A. SOLVING ($\overline{\text{P1}}$)

1) DUAL PROBLEM FOR ($\overline{\text{P1}}$)

Solving ($\overline{\text{P1}}$) is computationally prohibitive since the computational complexity is exponential in the number of subcarriers, so it is essential to decompose ($\overline{\text{P1}}$) into smaller parallel problems. The dual problem for ($\overline{\text{P1}}$) is formed by dualizing the total transmit power constraint and combining it with the objective function. Dualizing the total transmit power constraint makes the problem separable over the K subcarriers. Dual decomposition then allows one to evaluate the maximization on a per-subcarrier basis.

The Lagrange dual function is defined as

$$q(\boldsymbol{\alpha}, \hat{\boldsymbol{w}}_p, \hat{\boldsymbol{w}}_d, \lambda) \triangleq \max_{\mathsf{T},\mathsf{s}} \overline{\mathcal{L}}_1(\boldsymbol{\alpha}, \hat{\boldsymbol{w}}_p, \hat{\boldsymbol{w}}_d, \lambda, \mathsf{s}, \mathsf{T}) \tag{34}$$

where λ is the Lagrange multiplier for the total transmit power constraint and $\overline{\mathcal{L}}_1(\boldsymbol{\alpha}, \hat{\boldsymbol{w}}_p, \hat{\boldsymbol{w}}_d, \lambda, \mathsf{s}, \mathsf{T})$ is the Lagrangian. The Lagrangian may be expressed as

$$\begin{aligned}&\overline{\mathcal{L}}_1(\boldsymbol{\alpha}, \hat{\boldsymbol{w}}_p, \hat{\boldsymbol{w}}_d, \lambda, \boldsymbol{s}_k, \mathsf{T}_k)\\ &\quad = \lambda P_{\text{Total}} + \sum_{k=1}^{K} \overline{\mathcal{L}}_{1_k}^{\text{BC}}(\boldsymbol{\alpha}, \hat{\boldsymbol{w}}_p, \hat{\boldsymbol{w}}_d, \lambda, \boldsymbol{s}_k, \mathsf{T}_k),\end{aligned} \tag{35}$$

where

$$\begin{aligned}&\overline{\mathcal{L}}_{1_k}^{\text{BC}}(\boldsymbol{\alpha}, \hat{\boldsymbol{w}}_p, \hat{\boldsymbol{w}}_d, \lambda, \boldsymbol{s}_k, \mathsf{T}_k)\\ &\quad = \sum_{n=1}^{N} \hat{w}_{d_n} \hat{r}_{d_n} \; - \boldsymbol{t}_{k,n}^{\mathcal{H}} \Upsilon_k(\boldsymbol{\alpha}, \hat{\boldsymbol{w}}_p, \lambda) \boldsymbol{t}_{k,n} s_{k,n}\end{aligned} \tag{36}$$

and

$$\Upsilon_k(\boldsymbol{\alpha}, \hat{\boldsymbol{w}}_p, \lambda) = \left(\lambda \mathsf{I} - \sum_{m=1}^{N} \hat{w}_{p_m} (1 - \alpha_m) \boldsymbol{h}_{k,m} \boldsymbol{h}_{k,m}^{\mathcal{H}} \right). \tag{37}$$

Note that once λ is chosen, the maximization can be conducted independently on each subcarrier k. The Lagrange dual problem is then given by

$$\begin{aligned}\underset{\lambda}{\text{minimize}} \quad & q(\boldsymbol{\alpha}, \hat{\boldsymbol{w}}_p, \hat{\boldsymbol{w}}_d, \lambda)\\ \text{s.t.} \quad & \lambda \geq 0\\ & \Upsilon_k(\boldsymbol{\alpha}, \hat{\boldsymbol{w}}_p, \lambda) \succ 0 \; \forall k,\end{aligned} \tag{D1}$$

where the constraint on $\Upsilon_k(\boldsymbol{\alpha}, \hat{\boldsymbol{w}}_p, \lambda)$ ensures that (36) is bounded. The solution to the dual problem (D1) may then be defined as a function of the time-switching ratios. Let the solution to the dual problem (D1) for a given set of time-switching ratios be denoted with

$$\mathcal{D}_1(\boldsymbol{\alpha}, \hat{\boldsymbol{w}}_p, \hat{\boldsymbol{w}}_d) = \overline{\mathcal{L}}_1(\boldsymbol{\alpha}, \hat{\boldsymbol{w}}_p, \hat{\boldsymbol{w}}_d, \lambda^*, \mathsf{s}^*, \mathsf{T}^*), \tag{38}$$

where $\{\lambda^*, \mathsf{s}^*, \mathsf{T}^*\}$ are the optimal parameters given $\{\boldsymbol{\alpha}, \hat{\boldsymbol{w}}_p, \hat{\boldsymbol{w}}_d\}$.

2) MAC-BC DUALITY AND TRANSMIT POWER OPTIMIZATION

The MAC-BC duality theory used in this paper is similar to that developed in [32], [33], which is based on [34], [35], [36]. In [34], [35] it was shown that the per-subcarrier problem in the BC can be converted to an equivalent per-subcarrier problem in the MAC and was employed by [32], [33] for resource allocation in DSL networks. This duality may be used similarly to construct a MAC problem - referred to as the dual MAC - that has a solution linked to the solution of the BC problem ($\forall\, k$) in (34).

The duality between the per-subcarrier Lagrangian in the BC (36), denoted with $\overline{\mathcal{L}}_{1_k}^{\text{BC}}$, and the per-subcarrier Lagrangian in the dual MAC, denoted with $\overline{\mathcal{L}}_{1_k}^{\text{MAC}}$, is established and holds true for any T_k such that $\boldsymbol{t}_{k,n} \neq \boldsymbol{0}\; \forall\, n$ if [32], [33]:

1) For each dual MAC symbol power vector $\boldsymbol{\delta}_k \in \mathbb{R}_+^N$ a symbol power vector $\boldsymbol{s}_k \in \mathbb{R}_+^N$ exists such that $\overline{\mathcal{L}}_{1_k}^{\text{MAC}} = \overline{\mathcal{L}}_{1_k}^{\text{BC}}$ and $\gamma_{k,n}^{\text{MAC}}(\mathsf{T}_k, \boldsymbol{\delta}_k) = \gamma_{k,n}^{\text{BC}}(\mathsf{T}_k, \boldsymbol{s}_k)$, where $\gamma_{k,n}^{\text{MAC}}(\mathsf{T}_k, \boldsymbol{\delta}_k)$ denotes the dual MAC SINR and $\mathbb{R}_+^N$ denotes an $N \times 1$ vector of non-negative real numbers.
2) For each symbol power vector $\boldsymbol{s}_k \in \mathbb{R}_+^N$, a dual MAC symbol power vector $\boldsymbol{\delta}_k \in \mathbb{R}_+^N$ exists such that $\overline{\mathcal{L}}_{1_k}^{\text{BC}} = \overline{\mathcal{L}}_{1_k}^{\text{MAC}}$ and $\gamma_{k,n}^{\text{BC}}(\mathsf{T}_k, \boldsymbol{s}_k) = \gamma_{k,n}^{\text{MAC}}(\mathsf{T}_k, \boldsymbol{\delta}_k)$.

Hence, provided $\Upsilon_k(\boldsymbol{\alpha}, \hat{\boldsymbol{w}}_p, \lambda) \succ 0$, then for any precoder T_k and non-negative symbol power vector $\boldsymbol{s}_k$ in the BC there exists a dual MAC symbol power vector $\boldsymbol{\delta}_k$ that achieves the same SINR in the MAC (upstream channel H_k with equalizer $\mathsf{T}_k^{\mathcal{H}}$) as in the BC (downstream channel $\mathsf{H}_k^{\mathcal{H}}$ with precoder T_k) and vice versa [32], [33].

Converting the BC problem to a dual MAC problem begins with equating the SINRs

$$\gamma_{k,n}^{\text{BC}}(\mathsf{T}_k, \boldsymbol{s}_k) = \gamma_{k,n}^{\text{MAC}}(\mathsf{T}_k, \boldsymbol{\delta}_k) \; \forall\, k \text{ and } n \tag{39}$$

to satisfy the SINR requirement for establishing the duality, where $\gamma_{k,n}^{\text{BC}}(\mathsf{T}_k, \boldsymbol{s}_k)$ is defined in (3) and the dual MAC SINR is given by

$$\begin{aligned}&\gamma_{k,n}^{\text{MAC}}(\mathsf{T}_k, \boldsymbol{\delta}_k)\\ &\quad = \frac{|\boldsymbol{t}_{k,n}^{\mathcal{H}} \boldsymbol{h}_{k,n}|^2 \delta_{k,n}}{\sum_{\substack{m=1 \\ m \neq n}}^{N} |\boldsymbol{t}_{k,n}^{\mathcal{H}} \boldsymbol{h}_{k,m}|^2 \delta_{k,m} + \boldsymbol{t}_{k,n}^{\mathcal{H}} \Upsilon_k(\boldsymbol{\alpha}, \hat{\boldsymbol{w}}_p, \lambda) \boldsymbol{t}_{k,n}}.\end{aligned} \tag{40}$$

$\boldsymbol{\delta}_k$ is the $N \times 1$ dual MAC transmit power vector on subcarrier k and $\Upsilon_k(\boldsymbol{\alpha}, \hat{\boldsymbol{w}}_p, \lambda)$ is seen to act as a noise covariance matrix. Note that the equalizers in the dual MAC are also the precoders in the BC.

Since $\Upsilon_k(\boldsymbol{\alpha}, \hat{\boldsymbol{w}}_p, \lambda) \succ 0$, (39) may be expressed as:

$$\mathsf{Z}_k \boldsymbol{s}_k = \boldsymbol{\sigma}_k \circ \boldsymbol{\delta}_k \; \forall\, k, \tag{41}$$

where $\circ$ is the Hadamard product, $\boldsymbol{\sigma}_k$ is the vector of user noise power spectral densities for subcarrier k, and Z_k is given by:

$$\begin{aligned}[\mathsf{Z}_k]_{ij} &= \sum_{\substack{n=1 \\ n \neq j}}^{N} |\boldsymbol{t}_{k,j}^{\mathcal{H}} \boldsymbol{h}_{k,n}|^2 \delta_{k,n}\\ &\quad + \boldsymbol{t}_{k,j}^{\mathcal{H}} \Upsilon_k(\boldsymbol{\alpha}, \hat{\boldsymbol{w}}_p, \lambda) \boldsymbol{t}_{k,j}, \;\; \text{for } i = j\\ [\mathsf{Z}_k]_{ij} &= -\delta_{k,i} |\boldsymbol{t}_{k,j}^{\mathcal{H}} \boldsymbol{h}_{k,i}|^2, \;\; \text{for } i \neq j.\end{aligned} \tag{42}$$

Following the reasoning in [36], the inverse of Z_k only has non-negative elements because it is an M-matrix [37], so for any $\boldsymbol{\delta}_k \geq 0$, solving (41) will yield an $\boldsymbol{s}_k \geq 0$ and satisfies the symbol power non-negativity requirement for establishing the duality. Summing the rows of (41) yields:

$$\sum_{n=1}^{N} \boldsymbol{t}_{k,n}^{\mathcal{H}} \Upsilon_k\big(\boldsymbol{\alpha}, \hat{\boldsymbol{w}}_p, \lambda\big) \boldsymbol{t}_{k,n} s_{k,n} = \boldsymbol{\sigma}_k^{\mathcal{H}} \boldsymbol{\delta}_k, \tag{43}$$

which relates the BC precoders and transmit powers to the dual MAC transmit powers. The maximization problem ($\forall\ k$) in (34) may then be converted to the dual MAC by redefining the problem in terms of the dual MAC data rate and using (43) to arrive at:

$$\underset{\mathsf{T}_k, \boldsymbol{\delta}_k}{\text{maximize}}\ \overline{\mathcal{L}1}_k^{\text{MAC}}\big(\boldsymbol{\alpha}, \hat{\boldsymbol{w}}_p, \hat{\boldsymbol{w}}_d, \boldsymbol{\sigma}_k, \boldsymbol{\delta}_k, \mathsf{T}_k\big), \tag{44}$$

where

$$\begin{aligned} &\overline{\mathcal{L}1}_k^{\text{MAC}}\big(\boldsymbol{\alpha}, \hat{\boldsymbol{w}}_p, \hat{\boldsymbol{w}}_d, \boldsymbol{\sigma}_k, \boldsymbol{\delta}_k, \mathsf{T}_k\big) \\ &\quad = \sum_{n=1}^{N} \hat{w}_{d_n} \alpha_n \log_2\Big(1 + \gamma_{k,n}^{\text{MAC}}(\mathsf{T}_k, \boldsymbol{\delta}_k)\Big) - \boldsymbol{\sigma}_k^{\mathcal{H}} \boldsymbol{\delta}_k \end{aligned} \tag{45}$$

and establishes the duality between the BC and the dual MAC.

Equation (44) is separable when maximizing over T_k (given $\boldsymbol{\delta}_k$) since the SINR of user n (given by $\gamma_{k,n}^{\text{MAC}}$) only depends on the receive filter $\boldsymbol{t}_{k,n}$ of user n and $\boldsymbol{\sigma}_k^{\mathcal{H}} \boldsymbol{\delta}_k$ does not. This, along with the monotonicity of $\log_2(1+\cdot)$, allows one to only consider $\gamma_{k,n}^{\text{MAC}}(\mathsf{T}_k, \boldsymbol{\delta}_k)$ in the maximization:

$$\underset{\mathsf{T}_k}{\text{maximize}}\ \ \gamma_{k,n}^{\text{MAC}}(\mathsf{T}_k, \boldsymbol{\delta}_k). \tag{46}$$

The optimal linear equalizer for (46) is then the minimum mean square error (MMSE) linear equalizer because it maximizes received SINR [37]. Given the dual MAC SINR in (40), (46) can be cast as a maximization of a generalized Rayleigh quotient [38] and the linear MMSE equalizer is readily shown to be

$$\boldsymbol{t}_{k,n}^{*} = \left(\sum_{\substack{m=1 \\ m \neq n}}^{N} \delta_{k,m} \boldsymbol{h}_{k,m} \boldsymbol{h}_{k,m}^{\mathcal{H}} + \Upsilon_k\big(\boldsymbol{\alpha}, \hat{\boldsymbol{w}}_p, \lambda\big) \right)^{-1} \boldsymbol{h}_{k,n}. \tag{47}$$

The expression in (47) enables the dual MAC SINR to be expressed as only a function of $\boldsymbol{\delta}_k$,

$$\begin{aligned} &\gamma_{k,n}^{\text{MAC}}(\boldsymbol{\delta}_k) \\ &\quad = \delta_{k,n} \boldsymbol{h}_{k,n}^{\mathcal{H}} \left[\sum_{\substack{m=1 \\ m \neq n}}^{N} \delta_{k,m} \boldsymbol{h}_{k,m} \boldsymbol{h}_{k,m}^{\mathcal{H}} + \Upsilon_k\big(\boldsymbol{\alpha}, \hat{\boldsymbol{w}}_p, \lambda\big) \right]^{-1} \boldsymbol{h}_{k,n}. \end{aligned} \tag{48}$$

In turn, the maximization in (D1) can be further reformulated as only a function of the dual MAC transmit powers, where the per-subcarrier maximization is:

$$\underset{\boldsymbol{\delta}_k}{\text{maximize}} \sum_{n=1}^{N} \hat{w}_{d_n} \alpha_n \log_2\Big(1 + \gamma_{k,n}^{\text{MAC}}(\boldsymbol{\delta}_k)\Big) - \boldsymbol{\sigma}_k^{\mathcal{H}} \boldsymbol{\delta}_k. \tag{49}$$

The problem is still non-convex and successive convex approximation (SCA) may be employed to calculate the dual MAC transmit power, which entails optimizing the dual MAC transmit powers for one user at a time. For user n, this is done by first separating the cost function in (49) into $m = n$ and $m \neq n$ terms. Next, the dual MAC transmit powers $\delta_{k,m}$ for all $m \neq n$ are fixed constant and the respective dual MAC data rates are approximated with their first-order Taylor series expansion. The first-order Taylor series expansion takes the form of $f(x) = f(a) + f'(a)(x-a)$, where

$$\begin{aligned} a &= \bar{\boldsymbol{\delta}}_k \text{ and } x = \boldsymbol{\delta}_k \\ (x-a) &= \boldsymbol{\delta_k} - \bar{\boldsymbol{\delta}}_{\boldsymbol{k}} = \delta_{k,n} - \bar{\delta}_{k,n} \\ f(a) &= \sum_{\substack{m=1 \\ m \neq n}}^{N} \hat{w}_{d_m} \alpha_m \log_2\Big(1 + \gamma_{k,m}^{\text{MAC}}\big(\bar{\boldsymbol{\delta}}_k\big)\Big) - \boldsymbol{\sigma}_k^{\mathcal{H}} \bar{\boldsymbol{\delta}}_k \\ f'(a) &= \sum_{\substack{m=1 \\ m \neq n}}^{N} \frac{\hat{w}_{d_m} \alpha_m}{ln(2)} \frac{1}{1 + \gamma_{k,m}^{\text{MAC}}\big(\bar{\boldsymbol{\delta}}_k\big)} \frac{\partial \gamma_{k,m}^{\text{MAC}}\big(\bar{\boldsymbol{\delta}}_k\big)}{\partial \boldsymbol{\delta}_k} - \boldsymbol{\sigma}_k. \end{aligned} \tag{50}$$

Note that a is a known set of dual MAC transmit powers and x is the same except for the dual MAC transmit power for user n. After removing the constant terms and some additional manipulation, the problem simplifies to

$$\begin{aligned} \underset{\delta_{k,n}}{\text{maximize}}\quad & \hat{w}_{d_n} \alpha_n \log_2\big(1 + \delta_{k,n} \bar{q}_{k,n}\big) - \big(\bar{\phi}_{k,n} + \sigma_{k,n}\big) \delta_{k,n} \\ \text{s.t.}\quad & \delta_{k,n} \geq 0 \end{aligned} \tag{51}$$

where $\bar{q}_{k,n}$ is the interference-plus-noise covariance,

$$\bar{q}_{k,n} = \boldsymbol{h}_{k,n}^{\mathcal{H}} \left[\sum_{\substack{m=1 \\ m \neq n}}^{N} \bar{\delta}_{k,m} \boldsymbol{h}_{k,m} \boldsymbol{h}_{k,m}^{\mathcal{H}} + \Upsilon_k\big(\boldsymbol{\alpha}, \hat{\boldsymbol{w}}_p, \lambda\big) \right]^{-1} \boldsymbol{h}_{k,n}, \tag{52}$$

and $\bar{\phi}_{k,n}$ is from the first order Taylor series expansion of the data rates,

$$-\bar{\phi}_{k,n} = \frac{\partial}{\partial \delta_{k,n}} \left[\sum_{\substack{m=1 \\ m \neq n}}^{N} \hat{w}_{d_m} \alpha_m \log_2\Big(1 + \gamma_{k,m}^{\text{MAC}}(\boldsymbol{\delta}_k)\Big) \right] \Bigg|_{\boldsymbol{\delta}_k = \bar{\boldsymbol{\delta}}_k}. \tag{53}$$

Karush-Kuhn-Tucker (KKT) conditions enable calculating the optimal value for the dual MAC transmit power, $\delta_{k,n}$, by

taking the derivative of the cost function and setting it to 0, producing the following equation:

$$\delta_{k,n}^{*}=\left[0,\frac{\hat{w}_{d_n}\alpha_n}{\ln(2)\left(\bar{\phi}_{k,n}+\sigma_{k,n}\right)}-\frac{1}{\bar{q}_{k,n}}\right]^{+}, \tag{54}$$

where $[x,\ldots,y]^{+}=\max\{x,\ldots,y\}$. Applicable SCA algorithms with convergence results include block successive upper-bound minimization (BSUM) [39] and SJBR [40]. BSUM utilizes Gauss-Seidel updating to update a single dual MAC transmit power $\delta_{k,n}$ at a time. SJBR utilizes Jacobi updating to update an entire dual MAC transmit power vector $\boldsymbol{\delta}_k$. Both SCAs are implemented in Algorithm 1 in Section VI.

3) SOLVING THE DUAL PROBLEM

Problem (D1) is solved by adjusting the Lagrange multiplier until the total transmit power constraint is satisfied tightly. Since there is only one Lagrange multiplier, a simple bisection algorithm can be employed for this task. For every new λ, the resource allocation solves for the optimal dual MAC transmit powers given by (54) through SCA. Once a stationary point for the dual MAC transmit powers has been found, the equalizers for the dual MAC can be calculated via (47). The equalizers in the dual MAC are also the precoders in the BC, which may be used through (43) to calculate the transmit powers in the BC. If the resulting total power is not within the tolerance, then the Lagrange multiplier is adjusted and the process is repeated. Algorithm 2 in Section VI describes the complete resource allocation algorithm.

4) CONVEXITY, TIME-SHARING, AND THE DUALITY GAP

Problem ($\overline{\text{P1}}$) is not convex, so the duality gap may be non-zero. A non-zero duality gap implies that a solution to the dual problem does not necessarily produce an optimal solution for the primal problem. However, [9] discusses at length how the time-sharing property of multicarrier systems enables utilizing Lagrangian duality and dual decomposition for a problem in the form of ($\overline{\text{P1}}$), despite the non-convexity, and achieves a near-zero duality gap provided that the number of subcarriers is large enough. Practical multicarrier implementations (e.g. OFDM) require that the number of subcarriers is chosen to be large enough such that adjacent subcarriers experience similar fading characteristics that are nearly flat across the subcarrier [8], [9], thereby providing for a near-zero duality gap for a practical number of subcarriers. Simulations in [7] show that for a resource allocation scenario similar to that considered in this paper, an upper-bound for the duality gap relative to the feasible primal value decreased from less than $1e-3$ for $K=64$ to $7e-5$ for $K=512$. For $K=512$, [7] showed that this suboptimality amounted to a 0.296 bps /Hz summed bitrate density loss which is insignificant compared to the 4275.47 bps /Hz summed bitrate density achieved. Lastly, in practice, an algorithm usually terminates when the relative change in the objective value is less than some tolerance, where a reasonable tolerance may be on the order of $1e-3$. Thus, a gap of this magnitude (i.e., $1e-3$ or less) is immaterial in a practical system since the duality gap is within the convergence tolerance.

Algorithm 1 Inner Loop: SCA

Set convergence threshold, ϵ_δ
Set Method = SJBR or BSUM

function SCA($\hat{\boldsymbol{w}}_p, \hat{\boldsymbol{w}}_d, \boldsymbol{\alpha}, \lambda, \mathsf{H}, \boldsymbol{\sigma}$)
  for all $k \in \{1,\ldots,K\}$ **do** ▷ In parallel
    $\boldsymbol{\delta}_k \leftarrow 0$
    while Not Converged **do**
      $\boldsymbol{\delta}_k^{old} = \boldsymbol{\delta}_k$
      switch Method **do**
        case SJBR
        for all $n \in \{1,\ldots,N\}$ **do**
          Calculate $q_{k,n}$ using (52).
        for all $n \in \{1,\ldots,N\}$ **do**
          Calculate $\phi_{k,n}$ using (53).
        for all $n \in \{1,\ldots,N\}$ **do**
          Calculate $\delta_{k,n}$ using (54).
        case BSUM
        for all $m \in \{1,\ldots,N\}$ **do**
          for all $n \in \{1,\ldots,N\}$ **do**
            Calculate $q_{k,n}$ using (52).
          Calculate $\phi_{k,m}$ using (53).
          Calculate $\delta_{k,m}$ using (54).
      if $\frac{\|\boldsymbol{\delta}_k-\boldsymbol{\delta}_k^{old}\|}{\|\boldsymbol{\delta}_k+\boldsymbol{\delta}_k^{old}\|} \le \epsilon_\delta$ **then**
        Converged
    Calculate T_k based on (47).
    $\boldsymbol{s}_k \leftarrow \boldsymbol{\delta}_k$ using (43).
  return $\{\mathsf{T}, \mathsf{s}\}$

B. SOLVING ($\overline{\text{P2}}$) WITH LINEARIZED α-FAIRNESS

The precoding vectors need to be factorable to apply the MAC-BC duality, which is complicated by the non-linear utility functions in ($\overline{\text{P2}}$). Therefore this paper considers iteratively solving a linearized version of ($\overline{\text{P2}}$) given by ($\overline{\text{P1}}$) below. Next, the linearization will be developed for ($\overline{\text{P2}}$).

Problem ($\overline{\text{P2}}$) is non-convex. Yet through time-sharing, it was shown that these types of problems enjoy near-zero duality gaps that vanish asymptotically as the number of subcarriers goes to ∞, provided that the utility function is non-decreasing and concave [9]. By definition of α-fairness, f^{β} and $\hat{f}^{\beta}$ are non-decreasing and concave w.r.t. $\{r_{p_n}, r_{d_n}\}_{\forall n}$ and $\{\hat{r}_{p_n}, \hat{r}_{d_n}\}_{\forall n}$, respectively. Since the objectives are concave and the domain is convex due to time-sharing [9], [30], Problem ($\overline{\text{P2}}$) can be solved through the conditional gradient method [41] by linearizing and maximizing iteratively.

Algorithm 2 Resource Allocation for (P1)

Set the convergence tolerance, ϵ_p.
Set the total power constraint, P_{Total}.

function WSRPM($\hat{\boldsymbol{w}}_p, \hat{\boldsymbol{w}}_d, \boldsymbol{\alpha}$)
  Choose $\lambda_{\text{MIN}}, \lambda_{\text{MAX}}$
  $l = 0$, $P_l = \infty$
  while $\frac{|P_l - P_{\text{Total}}|}{P_{\text{Total}}} \geq \epsilon_p$ **do** ▷ Total Power Constraint
    $\lambda_l = (\lambda_{\text{MAX}} + \lambda_{\text{MIN}})/2$
    $\{\mathsf{T}_l, \mathsf{s}_l\} = \text{SCA}(\hat{\boldsymbol{w}}_p, \hat{\boldsymbol{w}}_d, \boldsymbol{\alpha}, \lambda_l, \mathsf{H}, \boldsymbol{\sigma})$
    Calculate p_{n_l} $\forall n$ with (5) then $P_l = \sum_n^N p_{n_l}$
    if $P_l < P_{\text{Total}}$ **then**
      $\lambda_{\text{MAX}} = \lambda_l$
    else
      $\lambda_{\text{MIN}} = \lambda_l$
    $l = l + 1$
  return $\{\mathsf{T}_l, \mathsf{s}_l, P_l, \lambda_l\}$

The linearized $\hat{f}^\beta$ is expressed as

$$\begin{aligned}\hat{f}^\beta_{\text{lin}} &\triangleq \sum_{n=1}^{N} \frac{\partial \hat{f}^\beta}{\partial \hat{r}_{p_n}}\bigg|_{\bar{r}_{p_n}} \left(\hat{r}_{p_n} - \bar{r}_{p_n}\right) + \frac{\partial \hat{f}^\beta}{\partial \hat{r}_{d_n}}\bigg|_{\bar{r}_{d_n}} \left(\hat{r}_{d_n} - \bar{r}_{d_n}\right) \\ &\quad + \hat{f}^\beta\left(\left\{\bar{r}_{p_n}, \bar{r}_{d_n}\right\}_{\forall n}\right) \\ &= \sum_{n=1}^{N} \frac{\hat{\mu}_{p_n}}{\left(\bar{r}_{p_n}\right)^\beta}\hat{r}_{p_n} + \frac{\hat{\mu}_{d_n}}{\left(\bar{r}_{d_n}\right)^\beta}\hat{r}_{d_n} + \text{Constant} \end{aligned} \tag{55}$$

where $\left\{\bar{r}_{p_n}, \bar{r}_{d_n}\right\}_{\forall n}$ is the set of data rates and harvested powers achieved in the previous iteration. "Constant" represents all terms that are independent of $\left\{\hat{r}_{p_n}, \hat{r}_{d_n}\right\}_{\forall n}$ and so do not affect the resource allocation. If this set is updated according to

$$\begin{aligned}\bar{r}_{d_{n_{j+1}}} &= (1 - \nu_j)\bar{r}_{d_{n_j}} + \nu_j \hat{r}_{d_{n_j}} \\ \bar{r}_{p_{n_{j+1}}} &= (1 - \nu_j)\bar{r}_{p_{n_j}} + \nu_j \hat{r}_{p_{n_j}}, \end{aligned} \tag{56}$$

while the step size ν is adjusted according to $\nu_j = 2/2+j$ then convergence is guaranteed [41]. Note that $\left\{\hat{r}_{p_{n_j}}, \hat{r}_{d_{n_j}}\right\}_{\forall n}$ is the solution in the j-th iteration. Observe that for $j = 0$, $\nu_j = 1$ and

$$\begin{aligned}\bar{r}_{d_{n_1}} &= \hat{r}_{d_{n_0}} \\ \bar{r}_{p_{n_1}} &= \hat{r}_{d_{n_0}}. \end{aligned} \tag{57}$$

In applying (55) we arrive at (P3)

$$\begin{aligned} \underset{\mathsf{T},\mathsf{s}}{\text{maximize}} \quad & \hat{f}^\beta_{\text{lin}} \\ \text{s.t.} \quad & \sum_{n=1}^{N} p_n \leq P_{\text{Total}} \\ & s_{k,n} \geq 0 \quad \forall\, k, n, \end{aligned} \tag{P3}$$

Omitting the constant term enables interpreting $\hat{f}^\beta_{\text{lin}}$ as a weighted sum, *equivalent* to (P1) with weights

$$\left\{\hat{w}_{p_{n_j}} = \frac{\hat{\mu}_{p_n}}{\left(\bar{r}_{p_{n_j}}\right)^\beta}, \hat{w}_{d_{n_j}} = \frac{\hat{\mu}_{d_n}}{\left(\bar{r}_{d_{n_j}}\right)^\beta}\right\}_{\forall n}. \tag{58}$$

Since α-Fairness utility functions are concave and the domain is convex due to time-sharing, successive linearization – where the problem is approximated by linear optimization for a series of points – should result in the globally optimal solution. Each linear problem is weighted by the tangent of the non-linear problem at the current iterate. When the tangent has zero slope, a critical point has been reached, which, for concave functions, is the global maximum. At this point, the linear problem can no longer improve the objective. Hence, (P2) can be solved iteratively through linearization by repeatedly solving (P1) for each update to the weights defined in (58). However, the underlying power allocation problem is still non-convex due to the nature of multiuser power allocations on individual subcarriers, so only a locally optimal solution is guaranteed. Since each subcarrier contributes only a small amount to the total objective, the suboptimality may be minor, especially if many subcarriers reach globally optimal solutions. Algorithm 3 implements (P2) by iteratively updating the weights in (58) and calling Algorithm 2 to perform the weighted sum maximization. In addition, as Proposition 3 shows, the linearization implies that the optimal time-switching ratio may be calculated using the weights defined in (58), the resulting resource allocation, and Lemma 2.

Proposition 3: The optimal time-switching ratio for the time-switched resource allocation corresponding to $\left\{\hat{r}_{p_n}, \hat{r}_{d_n}\right\}_{\forall n}$ that is optimal in (P3) for weights given in (58) is simultaneously given by

$$\alpha_n^* = \frac{\hat{\mu}_{d_n}\hat{r}_{d_n}}{\left(\bar{r}_{d_n}\right)^\beta}\left(\frac{\hat{\mu}_{p_n}\hat{r}_{p_n}}{\left(\bar{r}_{p_n}\right)^\beta} + \frac{\hat{\mu}_{d_n}\hat{r}_{d_n}}{\left(\bar{r}_{d_n}\right)^\beta}\right)^{-1} \tag{59}$$

and

$$1 - \alpha_n^* = \frac{\hat{\mu}_{p_n}\hat{r}_{p_n}}{\left(\bar{r}_{p_n}\right)^\beta}\left(\frac{\hat{\mu}_{p_n}\hat{r}_{p_n}}{\left(\bar{r}_{p_n}\right)^\beta} + \frac{\hat{\mu}_{d_n}\hat{r}_{d_n}}{\left(\bar{r}_{d_n}\right)^\beta}\right)^{-1}. \tag{60}$$

Proof: Solving (P3) is equivalent to iteratively solving (P1) with the weights defined in (58). Problem (P1) has an optimal time-switching ratio simultaneously defined in (17) and (16). Substituting the weights into (16) and (17) results in equations (60) and (59), respectively. ■

Note that if $\left\{\bar{r}_{p_n}, \bar{r}_{d_n}\right\}_{\forall n} = \left\{\hat{r}_{p_n}, \hat{r}_{d_n}\right\}_{\forall n}$ then Proposition 3 reduces to Proposition 1.

C. SOLVING (P2) WITH ALTERNATING OPTIMIZATION

The results from previous sections can now be used in combination with the AO. Let the search direction $\boldsymbol{d}_i$ for

Algorithm 3 α-Fairness: Resource Allocation for (P2)

Set the convergence tolerance, ϵ_β.

function AF_RA($\hat{\boldsymbol{\mu}}_p$,$\hat{\boldsymbol{\mu}}_d$,$\boldsymbol{\alpha}$,β)
  $j = 0$,$\hat{\boldsymbol{w}}_{p_j} = \hat{\boldsymbol{\mu}}_p$, $\hat{\boldsymbol{w}}_{d_j} = \hat{\boldsymbol{\mu}}_d$
  $\bar{r}_j = \left\{\bar{r}_{p_{n_j}}, \bar{r}_{d_{n_j}}\right\}_{\forall n} = \boldsymbol{0}$
  while true **do**
    $\{\mathsf{T}_j, \mathsf{s}_j, P_j, \lambda_j\}$ = WSRPM($\hat{\boldsymbol{w}}_{p_j}, \hat{\boldsymbol{w}}_{d_j}, \boldsymbol{\alpha}$)
    Generate $\left\{r_{p_{n_j}}, r_{d_{n_j}}\right\}$ using (6) and (8)
    Update $\nu_j = 2/2+j$
    Update $\bar{r}_{j+1} = \left\{\bar{r}_{p_{n_{j+1}}}, \bar{r}_{d_{n_{j+1}}}\right\}_{\forall n}$ using (56)
    ▷ Or (74) instead of (56)
    if $\|\frac{\bar{r}_{j+1}-\bar{r}_j}{\bar{r}_{j+1}+\bar{r}_j}\| \leq \epsilon_\beta$ **then**
      return $\{\hat{\boldsymbol{w}}_{p_j}, \hat{\boldsymbol{w}}_{d_j}, \boldsymbol{r}_{p_j}, \boldsymbol{r}_{d_j}, \mathsf{T}_j, \mathsf{s}_j, P_j, \lambda_j\}$
    $j = j + 1$
    Calculate $\hat{\boldsymbol{w}}_{p_j}$, $\hat{\boldsymbol{w}}_{d_j}$ from (58)

the time-switching ratios on iteration i, referred to as the *direction oracle*, be given by

$$\boldsymbol{d}_i = \boldsymbol{\alpha}_i^* - \boldsymbol{\alpha}_i, \tag{61}$$

where $\boldsymbol{\alpha}_i^*$ is calculated using Proposition 3. In the i-th iteration, the time-switching ratio may then be adjusted through

$$\boldsymbol{\alpha}_{i+1} = \boldsymbol{\alpha}_i + \nu_i \boldsymbol{d}_i, \tag{62}$$

which scales the step $\boldsymbol{d}_i$ by $\nu_i \in (0, 1]$. The maximum scaling is $\nu_i = 1$ since it sets the next iterate $\boldsymbol{\alpha}_{i+1} = \boldsymbol{\alpha}_i^*$, which is the time-switching ratio that makes the current resource allocation Pareto optimal on the Optimal RPR. The rationale for the direction oracle is illustrated in the Appendix A of [42] for a single-user scenario.

The direction oracle may be used here to solve (P̂2) by iteratively solving (P2) while adjusting the time-switching ratio. The time-switching ratio may be updated according to the iteration described with (62) in conjunction with Proposition 1. For each iteration of the time-switching ratio, (P2) may be solved by iteratively solving (P3) as a weighted sum through Algorithm 2. The step scaling ν is chosen such that the objective increases. Lemma 3 shows that $\hat{f}^\beta$ is concave w.r.t. the time-switching ratio and Lemma 4 proves that the direction oracle is an ascent direction for (P̂2). Hence, the step size scaling ν can be chosen as a square summable diminishing step size, through a backtracking line search that satisfies the Wolfe conditions, or set to a constant size less than the inverse of the Lipschitz constant. Theorem 1 proves that the iteration converges.

Lemma 3: The Hessian of $\hat{f}^\beta$ w.r.t. the time-switching ratio, $\nabla^2_{\boldsymbol{\alpha}} \hat{f}^\beta$, is negative definite, so $\hat{f}^\beta$ is strictly concave provided $0 < \alpha_n < 1$ and $\beta > 0$.

Proof: The gradient $\nabla_{\boldsymbol{\alpha}} \hat{f}^\beta$ for all values of β is a vector of partial derivatives given by

$$\frac{\partial}{\partial \alpha_n} \hat{f}^\beta = \frac{-\hat{\mu}_{p_n}}{(1-\alpha_n)^\beta \left(r_{p_n}\right)^{\beta-1}} + \frac{\hat{\mu}_{d_n}}{(\alpha_n)^\beta \left(r_{d_n}\right)^{\beta-1}}, \tag{63}$$

for all users n. The partial derivatives of the Hessian are given by

$$\frac{\partial^2}{\partial \alpha_n \partial \alpha_j} \hat{f}^\beta = \begin{cases} -\beta \left(\frac{\hat{\mu}_{p_n}}{(1-\alpha_n)^{\beta+1} \left(r_{p_n}\right)^{\beta-1}} + \frac{\hat{\mu}_{d_n}}{(\alpha_n)^{\beta+1} \left(r_{d_n}\right)^{\beta-1}} \right) & n = j \\ 0 & n \neq j. \end{cases} \tag{64}$$

All variables are positive, so $\nabla^2_{\boldsymbol{\alpha}} \hat{f}^\beta \prec 0$ for $\beta > 0$. Hence, $\hat{f}^\beta$ is strictly concave w.r.t. the time-switching ratio. ■

Lemma 4: The direction oracle defined in (61) is an ascent direction for (P̂2).

Proof: The sign of the i-th iteration of the direction oracle is given by

$$d_{n_i} = \alpha_{n_i}^* - \alpha_{n_i} : \begin{cases} > 0 & \alpha_{n_i} < \alpha_{n_i}^* \\ < 0 & \alpha_{n_i} > \alpha_{n_i}^* \\ 0 & \alpha_{n_i} = \alpha_{n_i}^* \end{cases} \forall n. \tag{65}$$

Proposition 1 can be used to determine the sign of the partial derivative of $\hat{f}^\beta$ for user n, derived in Lemma 3.

When $\alpha_{n_i}^* > \alpha_{n_i}$,

$$\begin{aligned} &\alpha_{n_i}^* > \alpha_{n_i} \\ &\frac{\hat{\mu}_{d_n}}{\left(\alpha_{n_i} r_{d_n}\right)^{\beta-1}} > \alpha_{n_i} \left(\frac{\hat{\mu}_{p_n}}{\left((1-\alpha_{n_i}) r_{p_n}\right)^{\beta-1}} + \frac{\hat{\mu}_{d_n}}{\left(\alpha_{n_i} r_{d_n}\right)^{\beta-1}} \right) \\ &\frac{\hat{\mu}_{d_n}}{\left(\alpha_{n_i}\right)^\beta \left(r_{d_n}\right)^{\beta-1}} > \frac{\hat{\mu}_{p_n}}{\left(1-\alpha_{n_i}\right)^\beta \left(r_{p_n}\right)^{\beta-1}}. \end{aligned} \tag{66}$$

When $\alpha_{n_i}^* < \alpha_{n_i}$,

$$\frac{\hat{\mu}_{d_n}}{\left(\alpha_{n_i}\right)^\beta \left(r_{d_n}\right)^{\beta-1}} < \frac{\hat{\mu}_{p_n}}{\left(1-\alpha_{n_i}\right)^\beta \left(r_{p_n}\right)^{\beta-1}}. \tag{67}$$

When $\alpha_{n_i}^* = \alpha_{n_i}$,

$$\frac{\hat{\mu}_{d_n}}{\left(\alpha_{n_i}\right)^\beta \left(r_{d_n}\right)^{\beta-1}} = \frac{\hat{\mu}_{p_n}}{\left(1-\alpha_{n_i}\right)^\beta \left(r_{p_n}\right)^{\beta-1}}. \tag{68}$$

Using the relations above, the sign of the partial derivative is given by

$$\frac{\partial}{\partial \alpha_n} \hat{f}^\beta : \begin{cases} > 0 & \alpha_{n_i} < \alpha_{n_i}^* \\ < 0 & \alpha_{n_i} > \alpha_{n_i}^* \\ 0 & \alpha_{n_i} = \alpha_{n_i}^*. \end{cases} \tag{69}$$

Since $\frac{\partial}{\partial \alpha_n} \hat{f}^\beta$ and d_{n_i} have the same sign for each case, $\boldsymbol{d}$ is an ascent direction. ■

Problem (P̂2) is solved via Algorithm 4, which can be found in Section VI. Theorem 1 will now prove that Algorithm 4 converges.

Theorem 1: Algorithm 4 converges to a solution for (P̂2).

Proof:

1) (P3) with weights (58) is an instance of (P1), for which [7] gives a converging algorithm.
2) (P2) has a concave objective and a domain that is convex due to time-sharing [9], [30], so it can be

solved through the conditional gradient method [41] by linearizing (P2) and iteratively maximizing. The linearization of (P2) results in (P3) which has a converging algorithm. Hence, (P2) can be solved by solving a sequence of problems in the form of (P3).

3) $\widehat{\text{(P2)}}$ is upper-bounded by a total transmit power constraint, so it can be solved through AO for $\widehat{\text{(P2)}}$ by using the direction oracle as an ascent step for $\widehat{\text{(P2)}}$ and using the converging algorithm for (P2).

Next, we will show that the $\mathcal{D}1$ iterates converge, hence so does Algorithm 4. For a fixed time-switching ratio, (P2) is solved iteratively by solving (P3) for each weight iterate. Each weight iterate is an ascent step, so

$$\mathcal{D}1\big(\boldsymbol{\alpha}, \hat{\boldsymbol{w}}_{p_{j+1}}, \hat{\boldsymbol{w}}_{d_{j+1}}\big) \geq \mathcal{D}1\big(\boldsymbol{\alpha}, \hat{\boldsymbol{w}}_{p_j}, \hat{\boldsymbol{w}}_{d_j}\big) \tag{70}$$

for all iterations j. Since (P2) is bounded from above by the total power constraint

$$\mathcal{D}1\Big(\boldsymbol{\alpha}, \hat{\boldsymbol{w}}_p^*, \hat{\boldsymbol{w}}_d^*\Big) \geq \mathcal{D}1\big(\boldsymbol{\alpha}, \hat{\boldsymbol{w}}_p, \hat{\boldsymbol{w}}_d\big) \tag{71}$$

where $\hat{\boldsymbol{w}}_p^*$ and $\hat{\boldsymbol{w}}_d^*$ are the optimal weights given $\boldsymbol{\alpha}$. Let it be clear that $\hat{\boldsymbol{w}}_p^*$ and $\hat{\boldsymbol{w}}_d^*$ are dependent on the value of $\boldsymbol{\alpha}$. Clearly $\mathcal{D}1$ will converge to a solution for (P2) given by $\mathcal{D}1(\boldsymbol{\alpha}, \hat{\boldsymbol{w}}_p^*, \hat{\boldsymbol{w}}_d^*)$.

Once (P2) is solved for a particular set of time-switching ratios, $\boldsymbol{\alpha}_i$, the time-switching ratios are also adjusted in the ascent direction, so

$$\mathcal{D}1\Big(\boldsymbol{\alpha}_{i+1}, \hat{\boldsymbol{w}}_{p_{i+1}}^*, \hat{\boldsymbol{w}}_{d_{i+1}}^*\Big) \geq \mathcal{D}1\Big(\boldsymbol{\alpha}_i, \hat{\boldsymbol{w}}_{p_i}^*, \hat{\boldsymbol{w}}_{d_i}^*\Big) \tag{72}$$

for all iterations i. Since the problem is bounded from above due to the total power constraint,

$$\mathcal{D}1\Big(\boldsymbol{\alpha}^{\text{opt}}, \hat{\boldsymbol{w}}_p^{\text{opt}}, \hat{\boldsymbol{w}}_d^{\text{opt}}\Big) \geq \mathcal{D}1\Big(\boldsymbol{\alpha}, \hat{\boldsymbol{w}}_p^*, \hat{\boldsymbol{w}}_d^*\Big), \tag{73}$$

where $\boldsymbol{\alpha}^{\text{opt}}$ is the optimal set of time-switching ratios and $\hat{\boldsymbol{w}}_p^{\text{opt}}$ and $\hat{\boldsymbol{w}}_d^{\text{opt}}$ are the associated optimal weights. Hence the iterates, and thus Algorithm 4, converge to the solution for $\widehat{\text{(P2)}}$ given by $\mathcal{D}1(\boldsymbol{\alpha}^{\text{opt}}, \hat{\boldsymbol{w}}_p^{\text{opt}}, \hat{\boldsymbol{w}}_d^{\text{opt}})$. ■

The above iteration waits for the convergence of (P2) before updating the time-switching ratio, so it may be slow to converge. Since the direction specified in (61) is an ascent direction for a given iterate and all values for the time-switching ratios are feasible, the time-switching ratio can be updated after each iterate. This can done by modifying (56) to

$$\begin{aligned}\bar{r}_{d_{n_{j+1}}} &= (1-\nu_j)\bar{r}_{d_{n_j}} + \nu_j \alpha_{n_{j+1}} r_{d_{n_j}} \\ \bar{r}_{p_{n_{j+1}}} &= (1-\nu_j)\bar{r}_{p_{n_j}} + \nu_j (1-\alpha_{n_{j+1}}) r_{p_{n_j}},\end{aligned} \tag{74}$$

where the update for $\boldsymbol{\alpha}_{j+1}$ is generated through (62). Adjusting the time-switching ratios in this way essentially amounts to changing Fixed-$\boldsymbol{\alpha}$ RPRs at each iteration, until it converges to the solution for $\widehat{\text{(P2)}}$.

Algorithm 4 α-Fairness: Optimal Time-Switching for $\widehat{\text{(P2)}}$

Set the convergence tolerance, ϵ_α.

function AF_OTSR($\hat{\boldsymbol{\mu}}_p$,$\hat{\boldsymbol{\mu}}_d$,$\boldsymbol{\alpha}$,β)
  $i = 0, \boldsymbol{\alpha}_i = \boldsymbol{\alpha}$
  while true **do**
    $\{\ldots\}_i = \text{AF_RA}\big(\hat{\boldsymbol{\mu}}_p, \hat{\boldsymbol{\mu}}_d, \boldsymbol{\alpha}_i, \beta\big)$
    Calculate $\boldsymbol{\alpha}_i^*$ using (59) or (77).
    Set ν_i, $\boldsymbol{\alpha}_{i+1} = \boldsymbol{\alpha}_i + \nu_i \boldsymbol{d}_i$
    if $\frac{\|\boldsymbol{\alpha}_{i+1} - \boldsymbol{\alpha}_i\|}{\|\boldsymbol{\alpha}_{i+1} + \boldsymbol{\alpha}_i\|} \leq \epsilon_\alpha$ **then**
      return $\{\hat{\boldsymbol{w}}_{p_i}, \hat{\boldsymbol{w}}_{d_i}, \boldsymbol{r}_{p_i}, \boldsymbol{r}_{d_i}, \mathsf{T}_i, \mathsf{s}_i, P_i, \boldsymbol{\alpha}_i\}$
    $i = i + 1$

D. OBSERVATIONS ON THE TIME-SWITCHING RATIO UPDATE

When iteratively solving $\widehat{\text{(P2)}}$ via (P2), an interesting relationship between the initial time-switching ratio and subsequent optimal time-switching ratio for the case of $\beta = 2$ is observed and described in Proposition 4.

Proposition 4: Suppose that (P2) for $\beta = 2$ is solved and an optimal time-switching ratio is calculated based on the resource allocation corresponding to $\{\hat{r}_{p_n}, \hat{r}_{d_n}\}_{\forall n}$. If this new time-switching ratio replaces the original time-switching ratio, the replaced point on the Optimal RPR will produce an equal objective value as the previous iteration.

Proof: Consider the objective for the time-switched version of (P2) with $\beta = 2$

$$\hat{f}^{\beta=2} = -\left(\sum_{n=1}^{N} \frac{\hat{\mu}_{p_n}}{\hat{r}_{p_n}} + \frac{\hat{\mu}_{d_n}}{\hat{r}_{d_n}}\right). \tag{75}$$

Assume that for the given weights $\{\hat{\mu}_{p_n}, \hat{\mu}_{d_n}\}_{\forall n}$ the optimal resource allocation corresponds to $\{\hat{r}_{p_n}, \hat{r}_{d_n}\}_{\forall n}$. The optimal time-switching ratio for this resource allocation is then calculated via (22) and (23) so that $\{\frac{1-\alpha_n^*}{1-\alpha_n}\hat{r}_{p_n}, \frac{\alpha_n^*}{\alpha_n}\hat{r}_{d_n}\}_{\forall n}$ lies on the Pareto edge of the Optimal RPR. Per this point, the objective of (75) is equal to

$$\begin{aligned}&\hat{f}^{\beta=2} \\ &= \sum_{n=1}^{N} \frac{-\hat{\mu}_{p_n}}{(1-\alpha_n^*) r_{p_n}} - \frac{\hat{\mu}_{d_n}}{\alpha_n^* r_{d_n}} \\ &= \sum_{n=1}^{N} \frac{-\hat{\mu}_{p_n}\left(\frac{\hat{\mu}_{pn}}{(1-\alpha_n) r_{p_n}} + \frac{\hat{\mu}_{d_n}}{\alpha_n r_{d_n}}\right)}{\hat{\mu}_{p_n} r_{p_n} / (1-\alpha_n) r_{p_n}} \\ &\qquad - \frac{\hat{\mu}_{d_n}\left(\frac{\hat{\mu}_{pn}}{(1-\alpha_n) r_{p_n}} + \frac{\hat{\mu}_{d_n}}{\alpha_n r_{d_n}}\right)}{\hat{\mu}_{d_n} r_{d_n} / \alpha_n r_{d_n}} \\ &= -\left(\sum_{n=1}^{N} \frac{\hat{\mu}_{p_n}}{r_{p_n}} + \frac{\hat{\mu}_{d_n}(1-\alpha_n)}{\alpha_n r_{d_n}} + \frac{\hat{\mu}_{d_n}}{r_{d_n}} + \frac{\hat{\mu}_{p_n}\alpha_n}{(1-\alpha_n) r_{p_n}}\right)\end{aligned}$$

$$= -\left(\sum_{n=1}^{N} \frac{\hat{\mu}_{p_n}}{(1-\alpha_n) r_{p_n}} + \frac{\hat{\mu}_{d_n}}{\alpha_n r_{d_n}}\right)$$
$$= -\left(\sum_{n=1}^{N} \frac{\hat{\mu}_{p_n}}{\hat{r}_{p_n}} + \frac{\hat{\mu}_{d_n}}{\hat{r}_{d_n}}\right). \tag{76}$$

Thus the objective of (75) is the same if the associated optimal time-switching ratio is used in place of the original time-switching ratio for $\{\hat{r}_{p_n}, \hat{r}_{d_n}\}_{\forall n}$. ■

Proposition 4 has the intriguing result that given a set of weights $\{\hat{\mu}_{p_n}, \hat{\mu}_{d_n}\}_{\forall n}$ (P2) will attain the same objective value for time-switching ratio iterates, provided that they are calculated via (62) with step size $\nu = 1$. Since $\nu = \{0, 1\}$ produces the same objective value, we surmise that any $\nu \in (0, 1)$ is an ascent step and that $0 < \nu < 1$ would make more progress. Notice that the concavity of $\hat{f}^{\beta}$ shown in Lemma 3 implies that the optimal time-switching ratio can be solved analytically. Proposition 5 derives the expression for the optimal time-switching ratio when solving (P2) for $\beta > 0$.

Proposition 5: For $\hat{f}^{\beta}$, the optimal value for the time-switching ratio is

$$\alpha_n^* = \left(1 + \sqrt[\beta]{\frac{\hat{\mu}_{p_n}}{\hat{\mu}_{d_n}} \left(\frac{r_{d_n}}{r_{p_n}}\right)^{\beta-1}}\right)^{-1} \tag{77}$$

for all $\beta > 0$ and for each user n.

Proof: Due to the concavity of $\hat{f}^{\beta}$ shown in Lemma 3, the optimal time-switching ratio can be solved analytically. The partial derivative of $\hat{f}^{\beta}$ w.r.t. α_n for all users n is given in (63). Setting the partial derivative to 0 and solving for the time-switching ratio

$$\frac{\hat{\mu}_{d_n}}{(\alpha_n)^{\beta}(r_{d_n})^{\beta-1}} = \frac{\hat{\mu}_{p_n}}{(1-\alpha_n)^{\beta}(r_{p_n})^{\beta-1}}$$
$$\left(\frac{1-\alpha_n}{\alpha_n}\right)^{\beta} = \frac{\hat{\mu}_{p_n}(r_{d_n})^{\beta-1}}{\hat{\mu}_{d_n}(r_{p_n})^{\beta-1}}$$
$$\frac{1-\alpha_n}{\alpha_n} = \sqrt[\beta]{\frac{\hat{\mu}_{p_n}(r_{d_n})^{\beta-1}}{\hat{\mu}_{d_n}(r_{p_n})^{\beta-1}}}$$
$$\alpha_n^* = \left(1 + \sqrt[\beta]{\frac{\hat{\mu}_{p_n}(r_{d_n})^{\beta-1}}{\hat{\mu}_{d_n}(r_{p_n})^{\beta-1}}}\right)^{-1}. \tag{78}$$

Since $0 \le \alpha_n^* \le 1$, the root is restricted to only the positive real solution. ■

Interestingly, when $\beta = 1$ Proposition 5 reduces to

$$\alpha_n^* = \left(1 + \sqrt[\beta]{\frac{\hat{\mu}_{p_n}(r_{d_n})^{\beta-1}}{\hat{\mu}_{d_n}(r_{p_n})^{\beta-1}}}\right)^{-1}\Bigg|_{\beta=1}$$
$$= \left(1 + \frac{\hat{\mu}_{p_n}}{\hat{\mu}_{d_n}}\right)^{-1}$$
$$= \frac{\hat{\mu}_{d_n}}{\hat{\mu}_{p_n} + \hat{\mu}_{d_n}}, \tag{79}$$

meaning that the optimal time-switching ratios are entirely defined by the weights. The implication is that in the algorithm, the optimization loop for the time-switching ratios disappears leaving only a linearization of the cost function.

VI. ALGORITHMS

A. DESCRIPTIONS

1) SOLVING (P1)

(P1) describes the problem of finding a resource allocation based on weights. It is solved through (D1), which is implemented in a nested loop comprised of an inner SCA, defined in Algorithm 1, and an outer bisection, defined in Algorithm 2.

Let ρ_k be the maximum eigenvalue of $\mathsf{H}_k^{\mathcal{H}} diag(\hat{\boldsymbol{w}}_p \circ (1 - \boldsymbol{\alpha}))\mathsf{H}_k$ on subcarrier k, where $\circ$ is the Hadamard product. Due to the constraint on $\Upsilon_k(\boldsymbol{\alpha}, \hat{\boldsymbol{w}}_p, \lambda)$, the lower bound λ_{MIN} for λ is given as

$$\lambda_{\text{MIN}} > [\rho_1, \ldots, \rho_K]^{+} = \rho_{\text{MAX}}. \tag{80}$$

The upper bound λ_{MAX} for λ is then any value $\lambda_{\text{MAX}} > \lambda_{\text{MIN}}$ that causes the total transmit power allocated by Algorithm 1 to be less than P_{Total}. Algorithm 2 first selects a Lagrange multiplier for the total power constraint based on the bounds $[\lambda_{\text{MIN}}, \lambda_{\text{MAX}}]$ and then calls Algorithm 1 to determine the dual MAC symbol power vector based on the chosen weights and the multiplier. Once the inner loop converges to the dual MAC symbol power vector, the precoding vectors are calculated, and in turn, so are the BC symbol power vectors. The precoding vectors and the BC symbol power vectors are passed back to the outer loop, Algorithm 2, where the total transmit power constraint is assessed for convergence and the algorithm iterates if necessary.

2) SOLVING (P2)

Algorithm 3 solves (P2) as described in Section V-B by linearizing the objective and iteratively solving it as a weighted sum using Algorithm 2.

3) SOLVING (P̂2)

Algorithm 4 makes use of Algorithm 3 by adjusting the time-switching ratio until the weights $\{\hat{w}_{p_n}, \hat{w}_{d_n}\}_{\forall n}$ produce a point on the Fixed-$\boldsymbol{\alpha}$ RPR that is tangent to the associated point on the Optimal RPR. At this point, the time-switching ratio is considered optimal for the given weights.

B. ASYMPTOTIC COMPUTATIONAL COMPLEXITY

Solving the primal problem to global optimality is computationally prohibitive due to its exponential complexity in the number of subcarriers; hence, decomposability is essential to render the problem tractable. Although the problem is non-convex–implying a generally non-zero duality gap–the time-sharing property of multicarrier systems ensures a zero duality gap under spectral continuity. As the number of subcarriers increases, spectral continuity improves, resulting in an asymptotically vanishing duality gap. Even with a

finite number of subcarriers, a near-zero duality gap can still be achieved when subcarriers experience flat fading and sufficient correlation–conditions inherently satisfied in practical OFDM systems due to the use of a cyclic prefix.

Furthermore, the orthogonality in OFDM ensures subcarrier independence, which enables the dual problem to decompose into simpler, parallelizable per-subcarrier problems. This is essential to reducing the complexity from exponential to linear in the number of subcarriers K. However, the presence of the time-switching ratios, which couple the subcarriers, prevents direct decomposition; thus, linearization is crucial to enabling dual decomposition in this context. The proposed method significantly reduces the computational complexity, especially for large K (e.g. $K = 1024$). The following sections analyze the asymptotic computational complexity of each algorithm component.

1) SCA

The symbol power and precoder vectors are calculated in the inner loop for each subcarrier k as described in Algorithm 1. Lagrangian decomposition allows these computations to be performed in parallel, yielding a linear dependence on K. The dominant computational cost per subcarrier arises from calculating $\bar{q}_{k,n}$ in (52), which involves a matrix inversion per user n. While direct inversion has complexity $O(N_T^3)$, this can be reduced to $O(N_T^2)$ using the Sherman–Morrison identity with rank-1 updates [43]. Therefore, the inner loop has per-iteration complexity $O(KN_T^2)$, and since the SCA typically converges in I_{SCA} iterations, the overall complexity becomes $O(KN_T^2 I_{\text{SCA}})$.

When BSUM is used for the SCA, the inner loop updates each user's power sequentially and requires N such updates per iteration. BSUM has been shown to converge sublinearly making the complexity $O(KN_T^2 N\epsilon_\delta^{-1})$, where ϵ_δ is the convergence tolerance [44]. In contrast, SJBR updates all user variables simultaneously and empirical results from [40] indicate that the required number of iterations is nearly constant and independent of ϵ_δ, typically $I_{\text{SCA}} \leq 10$. This leads to a total complexity of $O(KN_T^2)$.

2) POWER OPTIMIZATION

The power optimization step in $\overline{\text{P1}}$ involves a single total power constraint and is solved using the bisection algorithm in Algorithm 2. Bisection converges in $O(\log_2((\lambda_{\text{MAX}} - \rho_{\text{MAX}})\epsilon_p^{-1}))$ iterations [45], where ρ_{MAX} is the largest eigenvalue defined in (80), and ϵ_p is the power constraint tolerance.

3) α-FAIRNESS UTILITY

Algorithm 3 uses the conditional gradient method to optimize the resource allocation given $\{\hat{\mu}_{p_n}, \hat{\mu}_{d_n}\}_{\forall n}$, $\boldsymbol{\alpha}$, and β. It solves a sequence of linearized subproblems (solved using Algorithm 2) with diminishing step size, converging within $O(\epsilon_\beta^{-1})$ iterations [41], where ϵ_β is the convergence tolerance. The dominating component in each iteration is the in calculating the achieved harvested powers and data rates, with complexity $O(N^2K(N_T+1))$.

Algorithm 4 searches for the optimal time-switching ratio by iteratively calling Algorithm 3. It converges within $O(\epsilon_\alpha^{-1})$ iterations [46], where ϵ_α is the tolerance. If using (59), the asymptotic computational complexity for each iteration is $O(N\ln(\beta))$ whereas if using (77), it is $O(N\ln(\beta)\ln(\beta-1))$. Note that the complexity can be further improved by using the update defined in (74), which updates the time-switching ratios with each iteration of Algorithm 3. This reduces the time complexity from $O(\epsilon_\beta^{-1}\epsilon_\alpha^{-1})$ to within the range of $[O(\epsilon_\beta^{-1}), O(\epsilon_\beta^{-1}\epsilon_\alpha^{-1})]$.

4) TOTAL ASYMPTOTIC COMPUTATIONAL COMPLEXITY

The total asymptotic complexity depends on the algorithm choices. The minimum asymptotic computational complexity occurs when using SJBR for SCA, (74) is used for the linearization, and (59) for time-switching updates. The total complexity is:

$$O\left(K^2N^3N_T^2(N_T+1)\ln\beta\log_2((\lambda_{\text{MAX}}-\rho_{\text{MAX}})\epsilon_p^{-1})\epsilon_\beta^{-1}\right)$$

The maximum asymptotic computational complexity occurs when using BSUM for SCA, (56) is used for the linearization, and (77) for the time-switching updates. The complexity becomes:

$$O\left(K^2N^4N_T^2(N_T+1)\ln\beta\log_2((\lambda_{\text{MAX}}-\rho_{\text{MAX}})\epsilon_p^{-1})\epsilon_\beta^{-1}\ln(\beta-1)\epsilon_\delta^{-1}\epsilon_\alpha^{-1}\right)$$

In any case, the overall complexity transitions from exponential to polynomial in problem size, representing a significant improvement over globally optimal solutions.

VII. SIMULATIONS

The cyclic prefix in OFDM is a buffer prepended to the time-domain data, consisting of the last γ samples of the data intended for transmission. The length of the cyclic prefix is required to be equal to or greater than the length of the channel's impulse response in samples. If the total number of data time-domain samples is K, then OFDM necessitates that $K \geq \gamma$ to ensure a sufficient number of samples are available to form the cyclic prefix. Since a K-point FFT results in K subcarriers (i.e.,, channel coefficients), the length requirement for the cyclic prefix places a lower bound on the number of subcarriers, i.e., $K \geq \gamma$. In turn, this lower bound requires that the inverse of the subcarrier spacing is equal to or greater than the channel impulse response and ensures that the subcarrier spacing is approximately equal to or less than the coherence bandwidth [48], resulting in subcarriers with relatively flat fading characteristics.

For the following simulations, the MISO channel matrices H_k for all subcarriers k are generated using the MATLAB Communications Toolbox [49], based on the settings in Table 1 and a tapped delay line model [50] for a Rayleigh fading environment as specified in [47]. Table 2 shows that $K = 64$ and the system bandwidth is 20MHz, which, based on the simulations in [7], satisfies the OFDM subcarrier spacing requirements for this channel. If the entire impulse

TABLE 1. MIMOChannel toolbox settings.

Parameter	Value
'SampleRate'	20 MHz
'SpatialCorrelationSpecification'	'None'
'NumTransmitAntennas'	N_T
'NumReceiveAntennas'	N
'FadingDistribution'	'Rayleigh'
'MaximumDopplerShift'	0
'NormalizeChannelOutputs'	true
'AntennaSelection'	'Tx and Rx'

TABLE 2. System parameters.

Parameter	Value
Number of Subcarriers, K	64
OFDM System Bandwidth	20 MHz
Subcarrier Spacing	312.5 kHz
Total Power Constraint, P_{Total}	30 dBm
Large Scale Pathloss	60 dB
Number of Transmit Antennas, N_{T}	6 or 10
Number of Users, N	2 or 4
Tolerance, ϵ_α	10^{-2}
Tolerance, ϵ_β	10^{-4}
Tolerance, ϵ_p	10^{-7}
Tolerance, ϵ_δ	10^{-10}
Fading Environment	Rayleigh [47]
Noise Power Density,σ	-112 dBm/Hz
Weights, $\{\hat{\mu}_{p_n}, \hat{\mu}_{d_n}\}_{\forall n}$	Listed in the figure caption.

response is captured within K time-domain samples, a K-point FFT can determine the channel coefficients for subcarriers with sufficient spacing. The channel impulse response is calculated for each transmit-receive antenna pair, and a K-point FFT is applied to obtain the individual channel vectors $\boldsymbol{h}_{k,n}$ for each subcarrier k and user n. The resulting channel coefficients reflect the correlated multipath effects, which is critical for the time-sharing property to hold, for all propagation paths between each transmit and receive antenna.

Since the optimality of the underlying resource allocation method has already been established in [7] - applied through the linearization in Section V-B - and likewise for the time-switching ratio optimization in [26], the simulations in this manuscript primarily serve to illustrate that (i) the developed approaches converge to similar solutions consistent with those of the prior methods and (ii) fairness is effectively incorporated into the resource allocation and (iii) to illustrate the observations made in Section V-D.

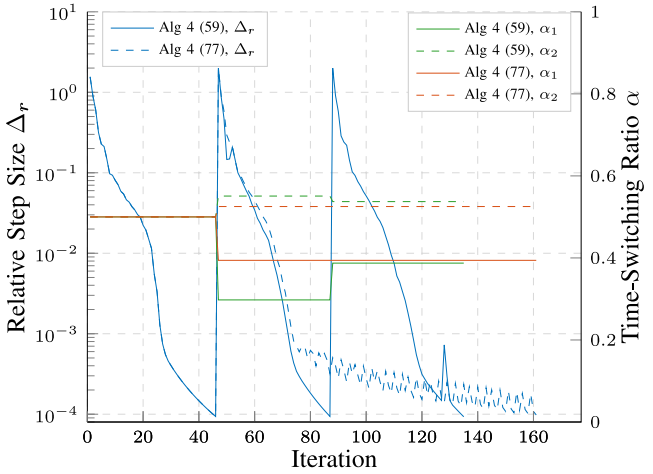

FIGURE 4. The progress of Algorithm 4 w.r.t. iteration while optimizing the time-switching ratios through (59) or (77) with a diminishing square summable step size. $N_T = 6$, $N = 2$, $\hat{\mu}_p = [2, 1]^\top$, $\hat{\mu}_d = [1, 2]^\top$, initial $\alpha = [0.5, 0.5]^\top$, and $\beta = 2$.

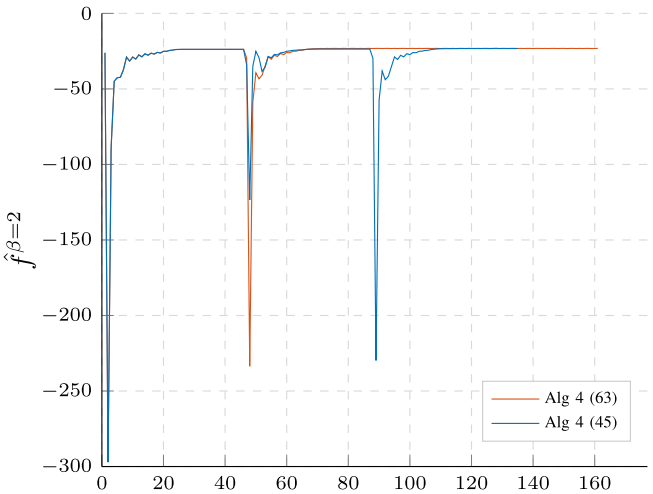

FIGURE 5. The objective value of Algorithm 4 w.r.t. iteration while optimizing the time-switching ratios through (59) or (77) with a diminishing square summable step size. $N_T = 6$, $N = 2$, $\hat{\mu}_p = [2, 1]^\top$, $\hat{\mu}_d = [1, 2]^\top$, initial $\alpha = [0.5, 0.5]^\top$, and $\beta = 2$.

A. CONVERGENCE BEHAVIOR AND INFLUENCE OF β ON SUBCARRIER POWER ALLOCATION

This subsection presents the simulation results that highlight the convergence behavior and the influence of fairness parameters on subcarrier power allocation in the transmit and receive domains. Figs. 4 and 6 demonstrate the convergence of the relative step size and time-switching ratios, with Algorithm 3 showing faster convergence. Figs. 5 and 7 illustrate utility maximization, where Algorithm 3 makes better progress due to iterative adjustments of both resource allocation and time-switching ratios. Fig. 8 shows rapid convergence of user objectives within 25 iterations using Algorithm 3. Figs. 9-12 compare transmit and received power allocations for fairness parameters $\beta = 1$ and $\beta = 5$, revealing more equitable power distribution with higher fairness. Lastly, Figs. 13 and 14 illustrate how increased

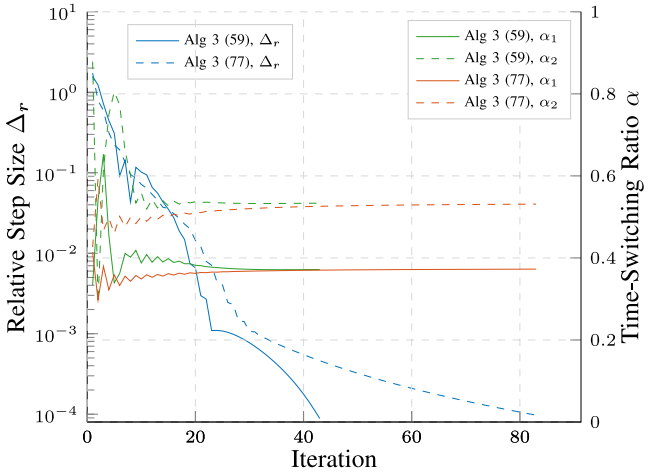

FIGURE 6. The progress of Algorithm 3 w.r.t. iteration while optimizing the time-switching ratios using update (74), (59) or (77), and with a diminishing square summable step size. $N_T = 6$, $N = 2$, $\hat{\mu}_p = [2, 1]^\top$, $\hat{\mu}_d = [1, 2]^\top$, initial $\alpha = [0.5, 0.5]^\top$, and $\beta = 2$.

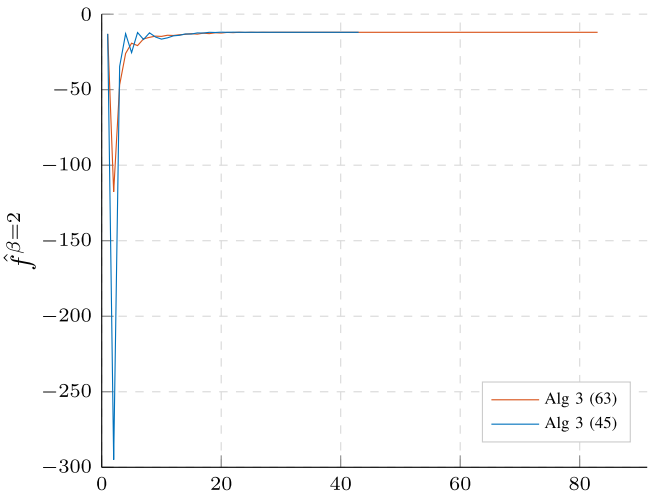

FIGURE 7. The objective value of Algorithm 3 w.r.t. iteration while optimizing the time-switching ratios using update (74), (59) or (77), and with a diminishing square summable step size. $N_T = 6$, $N = 2$, $\hat{\mu}_p = [2, 1]^\top$, $\hat{\mu}_d = [1, 2]^\top$, initial $\alpha = [0.5, 0.5]^\top$, and $\beta = 2$.

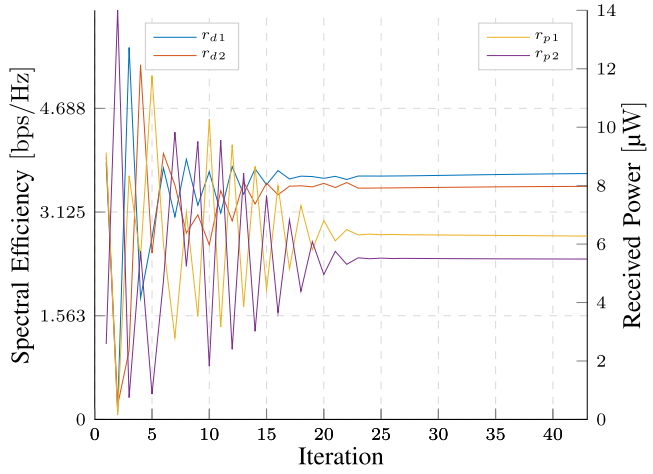

FIGURE 8. Algorithm 3 (using update (74) and (59)) alternates between updating the data rate and received power allocation $\{r_{pn}, r_{dn}\}_{\forall n}$ and updating the time-switching ratios. Here the $\{r_{pn}, r_{dn}\}_{\forall n}$ iterates are illustrated showing convergence within 45 iterations. Algorithm 3 parameters include a diminishing square summable step size, $N_T = 6$, $N = 2$, $\hat{\mu}_p = [2, 1]^\top$, $\hat{\mu}_d = [1, 2]^\top$, initial $\alpha = [0.5, 0.5]^\top$, and $\beta = 2$.

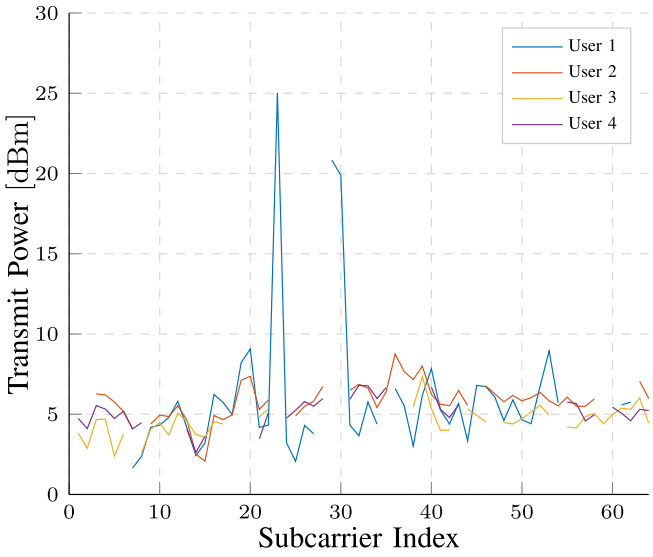

FIGURE 9. The subcarrier transmit power allocation from Algorithm 3 (using update (74) and (59)) is illustrated for all users. Observe that user 1 is allocated more power due to having the largest harvested power weight $\hat{\mu}_{p_1} = 2$ and user 2 was allocated power over the most subcarriers due to having the largest data rate weight $\hat{\mu}_{d_2} = 2$. Note that power is allocated only to one user on subcarriers that are interference limited (e.g. user 1). The parameters include a diminishing square summable step size, $N_T = 6$, $N = 4$, $\hat{\mu}_p = [2, 1, 1, 1]^\top$, $\hat{\mu}_d = [1, 2, 1, 1]^\top$, initial $\alpha = [0.9, 0.1, 0.25, 0.75]^\top$, and $\beta = 1$.

fairness compresses the range of time-switching ratios, resulting in more balanced resource allocations across users.

It was noted that Algorithm 4 may take a relatively long time to converge since it requires a solution for (P2) before it can adjust the time-switching ratios. For a 2 user network, Fig. 4 shows the relative step size of the resource allocation, denoted with $\Delta_{\boldsymbol{r}}$, w.r.t. the iteration number for Algorithm 4. $\Delta_{\boldsymbol{r}}$ is given by line 10 in Algorithm 3. The time-switching ratios are updated through a diminishing step size, using either (59) or (77). Both take over 100 iterations to converge, but (77) took the longest. Although it started converging earlier than the other formula at approximately iteration 70. Fig. 6 also shows the relative step size of the resource allocation iterates w.r.t. the iteration number, but for Algorithm 3 when using (74) as the iterate update. Both methods for choosing the time-switching ratios converge faster than in Algorithm 4 and (59) was the quickest. Algorithm 3 had tighter convergence tolerances, using ϵ_β, than Algorithm 4, which used ϵ_α. However, Algorithm 3 still converged more quickly. All methods result in similar resource allocations and time-switching ratios. The time-switching ratios in Algorithm 3 converged to $\boldsymbol{\alpha} = [0.3718, 0.5335]^\top$ and, in Algorithm 4, $\boldsymbol{\alpha} = [0.38736, 0.5373]^\top$ for (59) and $\boldsymbol{\alpha} = [0.39412, 0.5253]^\top$ for (77). The maximization of the utility objective value is illustrated for Algorithm 4 in Fig. 5 and Algorithm 3 in Fig. 7. Both attained similar objective values, but because Algorithm 3 alternates between adjusting the

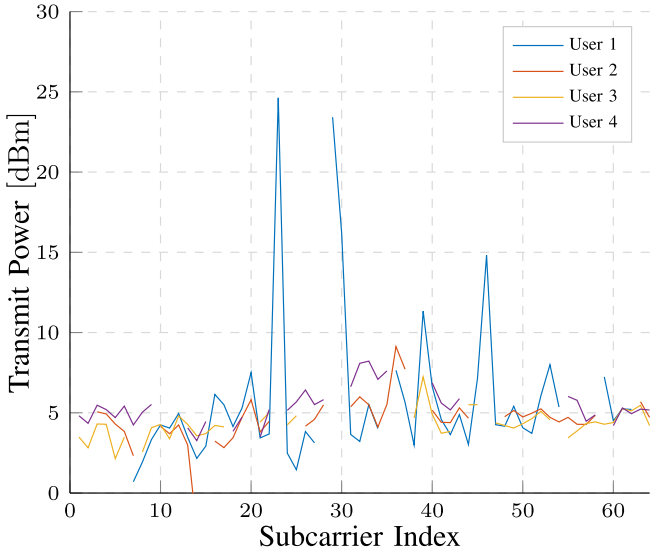

FIGURE 10. The fairness parameter is increased to $\beta = 5$, causing Algorithm 3 (using update (74) and (59)) to redistribute transmit power to promote power delivery to the other user 2,user 3, and user 4 while also promoting higher data rates for user 1, user 3, and user 4. Observe that power allocated to user 1 on subcarriers $k = 23$ and $k = 30$ has been reallocated to $k \in [29, 39, 46, 59]$. The parameters include a diminishing square summable step size, $N_T = 6$, $N = 4$, $\hat{\mu}_p = [2, 1, 1, 1]^\top$, $\hat{\mu}_d = [1, 2, 1, 1]^\top$, initial $\alpha = [0.9, 0.1, 0.25, 0.75]^\top$, and $\beta = 5$.

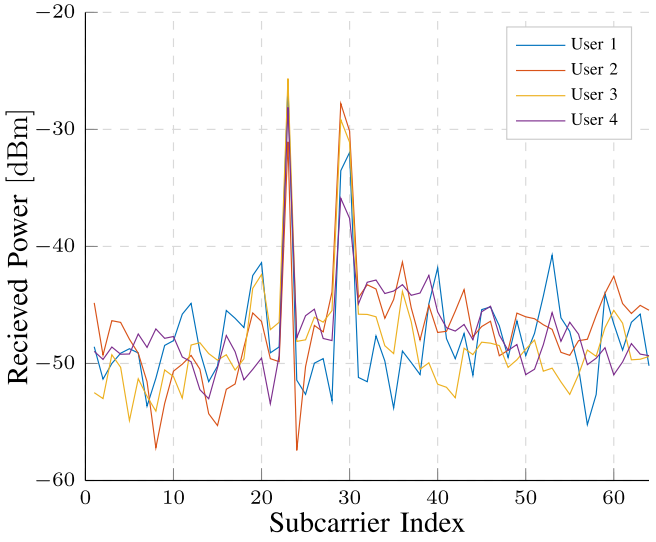

FIGURE 11. Subcarrier received power allocation for $N_T = 6$, $N = 4$, $\hat{\mu}_p = [2, 1, 1, 1]^\top$, $\hat{\mu}_d = [1, 2, 1, 1]^\top$, initial $\alpha = [0.9, 0.1, 0.25, 0.75]^\top$, and $\beta = 1$.

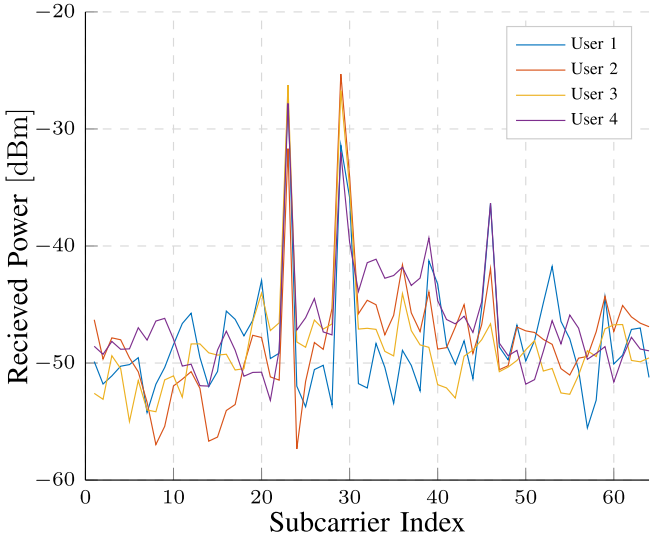

FIGURE 12. The fairness parameter is increased to $\beta = 5$, causing the received power allocation to improve for the users with lower priorities (i.e., user 2, user 3, and user 4). The simulation used a diminishing step size, $N_T = 6$, $N = 4$, $\hat{\mu}_p = [2, 1, 1, 1]^\top$, $\hat{\mu}_d = [1, 2, 1, 1]^\top$, initial $\alpha = [0.9, 0.1, 0.25, 0.75]^\top$, and $\beta = 5$.

resource allocation and the time-switching ratios for every iteration it has more opportunity to tune the time-switching ratios in conjunction with the resource allocation and so made better progress than Algorithm 4. Fig. 8 shows the convergence of the non-time-switched resource allocation for Algorithm 3 using (59). The remaining simulations in Section VII-A will only use Algorithm 3 with update (74) and (59).

Fig. 9 illustrates the resulting transmit power allocation w.r.t. the subcarrier index for 4 users with $\beta = 1$. There are large spikes in power allocated to user 1 at roughly $k \in \{23, 29, 30\}$, which is due to user 1 having the highest harvested power priority, $\hat{\mu}_{p_1} = 2$. Notice that these subcarriers only have power allocated to a single user. This is because the individual subcarriers are interference-limited due to the high power allocation for user 1. In order to mitigate the interference the system must either suppress it through precoding or assign the subcarrier to one user, which in this case assigned the subcarrier to user 1. Note, however, that this subcarrier assignment does not preclude the other users from harvesting interference received on this subcarrier. In terms of the number of subcarriers allocated to each user for data transfer, user 1 has 49, user 2 has 52, user 3 has 41, and user 4 has 38. This allocation is influenced by multiple things including the data rate weights, which user 2's was the largest with $\hat{\mu}_{d_2} = 2$.

Increasing the fairness parameter to $\beta = 5$ results in the transmit power allocation illustrated in Fig. 10. Comparing Fig. 9 to Fig. 10, it can be seen that some power was reallocated from subcarriers $k \in [1, 23]$ and $k \in [50, 64]$ to subcarriers $k \in [29, 49]$. Increasing the fairness value decreased the number of subcarriers allocated to user 2, which had the highest data rate weight, and increased the number of subcarriers allocated to the other users. Specifically, the number of subcarriers allocated to user 1 increased to 51, user 2 decreased to 46, user 3 increased to 44, and user 4 increased to 41. According to the well-known Shannon-Hartley theorem, channel capacity is linearly related to the amount of bandwidth so this reallocation of subcarriers ostensibly decreased the data rate for user 2 while increasing the data rates for the other users and thus increased the data rate allocation fairness.

Fig. 11 illustrates the received power (i.e.,, power captured by the receive antenna) for $\beta = 1$. Notice how all users are able to harvest some power from each subcarrier, even if the

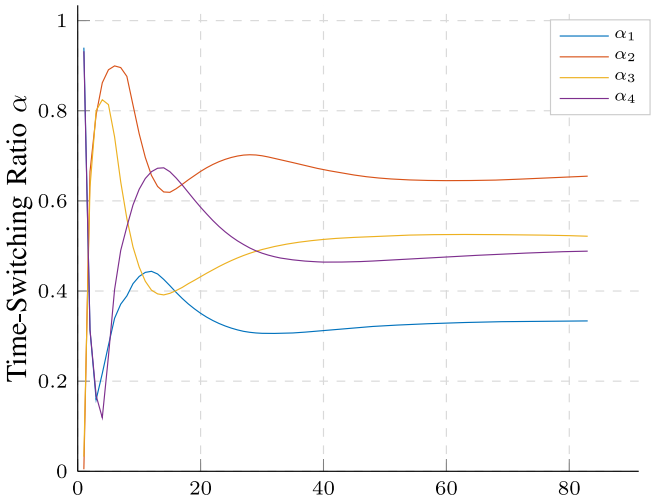

FIGURE 13. Algorithm 3 while optimizing the time-switching ratios through (74) and (59) with a diminishing square summable step size. $N_T = 6$, $N = 4$, $\hat{\mu}_p = [2, 1, 1, 1]^\top$, $\hat{\mu}_d = [1, 2, 1, 1]^\top$, initial $\alpha = [0.9, 0.1, 0.25, 0.75]^\top$, and $\beta = 1$.

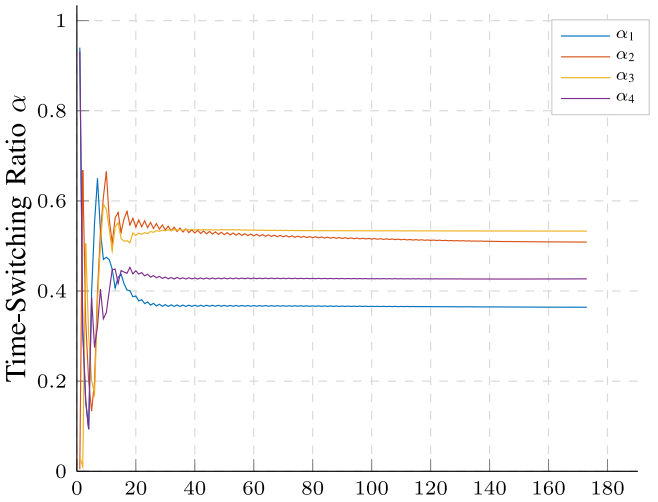

FIGURE 14. Algorithm 3 while optimizing the time-switching ratios through (74) and (59) with a diminishing square summable step size. $N_T = 6$, $N = 4$, $\hat{\mu}_p = [2, 1, 1, 1]^\top$, $\hat{\mu}_d = [1, 2, 1, 1]^\top$, initial $\alpha = [0.9, 0.1, 0.25, 0.75]^\top$, and $\beta = 5$.

power is allocated to certain users (i.e., interference power is harvested). Fig. 12 shows the impact of increasing the fairness parameter to $\beta = 5$ on the received power. As in the transmit power allocation for $\beta = 5$, subcarriers $k \in [0, 23]$ and $k \in [50, 64]$ generally lost power while $k \in [29, 49]$ had an increase in received power. This resulted in the received power increasing on $k = 29$ for users 2 - 4, on $k = 39$ for user 2 and 4, on $k = 46$ for all users, and for user 3 on $k = 59$. Hence, the harvested power allocation fairness increased.

The convergence of the time-switching ratios for $\beta = 1$ is illustrated in Fig. 13. It shows that the time-switching ratio for user 1 converges to $\alpha_1 = 0.3336$, which is a value that supports higher harvested power and is inline with its higher priority (i.e., $\hat{\mu}_{p_1} > \hat{\mu}_{p_{2,3,4}}$), and user 2 attained a time-switching ratio $\alpha_2 = 0.6548$, which is a value that supports higher data rates inline with its higher priority (i.e., $\hat{\mu}_{d_2} > \hat{\mu}_{d_{1,3,4}}$). Both user 3 and user 4 had equal weights $\hat{\mu}_{p_{3,4}} = \hat{\mu}_{d_{3,4}} = 1$ and their time-switching ratios converged to similar mid-level values, $\alpha_3 = 0.5215$ and $\alpha_4 = 0.4884$. Also note that since $\beta = 1$, (79) may be used to calculate the optimal time-switching ratios purely based on the time-switched weights resulting in $\boldsymbol{\alpha}^* = [0.3333, 0.666, 0.5, 0.5]^\top$. The relative error for the converged time-switching ratios can then be calculated as $|\boldsymbol{\alpha} - \boldsymbol{\alpha}^*| \oslash \boldsymbol{\alpha}^* = [9\text{e}{-4}, 0.0177, .043, 0.0232]^\top$, where $\oslash$ is Hadamard division, and shows close agreement.

In Fig. 14 the fairness parameter is increased to $\beta = 5$. It shows that the time-switching ratio for user 1 converges to $\alpha_1 = 0.3640$, which is little larger but is still a value that supports higher harvest power, user 2 attained a time-switching ratio $\alpha_2 = 0.5086$, which is significantly lower and is now mid-level, user 3 at $\alpha_3 = 0.5329$ stayed roughly the same, and user 4 decreased to $\alpha_4 = 0.4269$. With an increased β, equity in the objectives becomes more important. Based on the changes of the time-switching ratios it appears that the system sacrificed some data rate to increase the amount of power harvested.

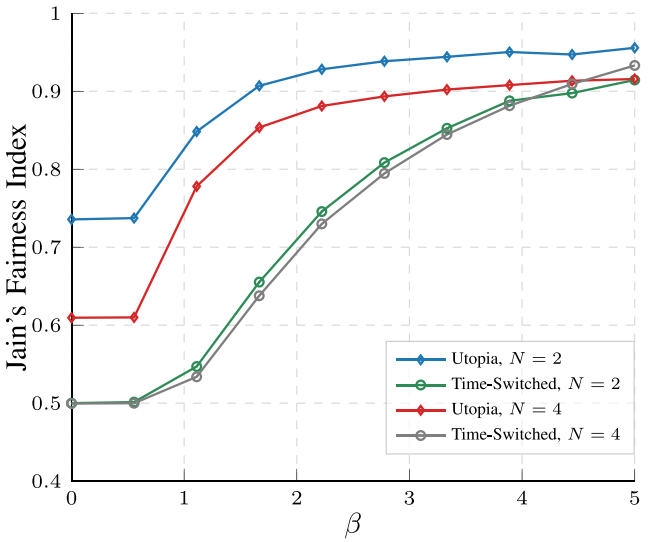

FIGURE 15. Jain's fairness index as a function of the fairness parameter β for the Utopia point and the time-switched point. All elements in $\hat{\mu}_p$ are set to 1 and all elements in $\hat{\mu}_d$ are set to 10. The optimal time-switching ratios were calculated using Proposition 5. The parameters used include a diminishing square summable step size, $N = 4$ or $N = 2$, and $N_T = 10$.

B. EFFECT OF THE FAIRNESS PARAMETER ON THE RESOURCE ALLOCATION

This subsection presents the simulation results that demonstrate the effect of the fairness parameter β on resource allocations in a system with user weights chosen to promote unfairness, in this case high data rates for all users. Fig. 15 illustrates that fairness improves as β increases from 0 to 5. The Utopia points saturate earlier than the time-switched points, indicating that improved fairness is first achieved

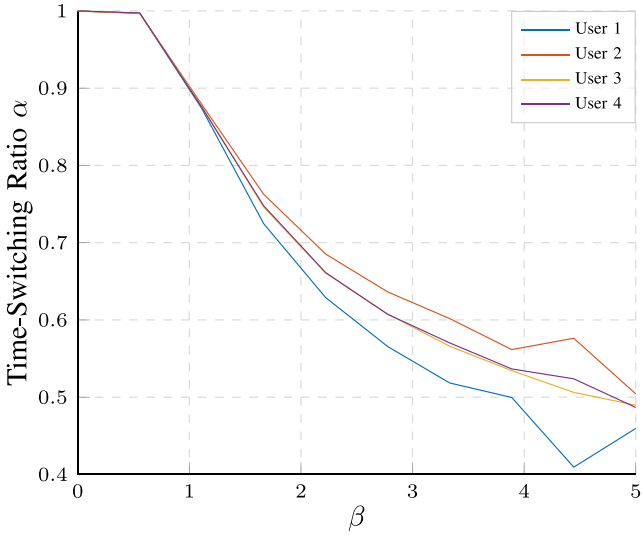

FIGURE 16. Time-switching ratio with respect to β for $N_T = 10$ and $N = 4$. All elements in $\hat{\mu}_p$ are set to 1 and all elements in $\hat{\mu}_d$ are set to 10.

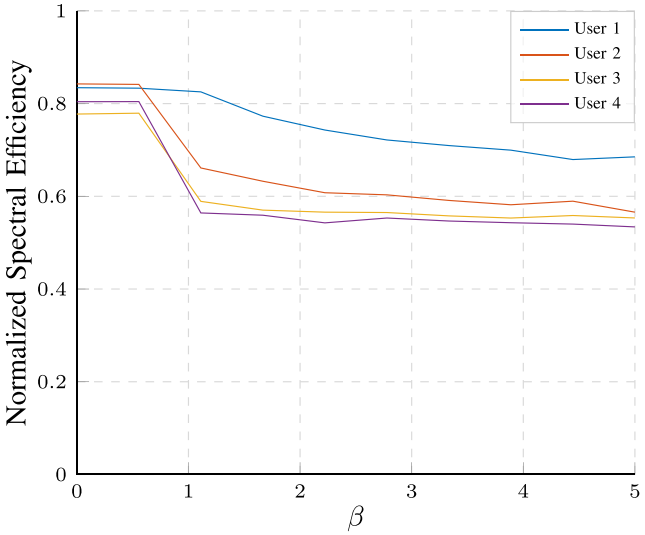

FIGURE 17. Normalized utopia data rates w.r.t. β for $N_T = 10$ and $N = 4$. All elements in $\hat{\mu}_p$ are set to 1 and all elements in $\hat{\mu}_d$ are set to 10.

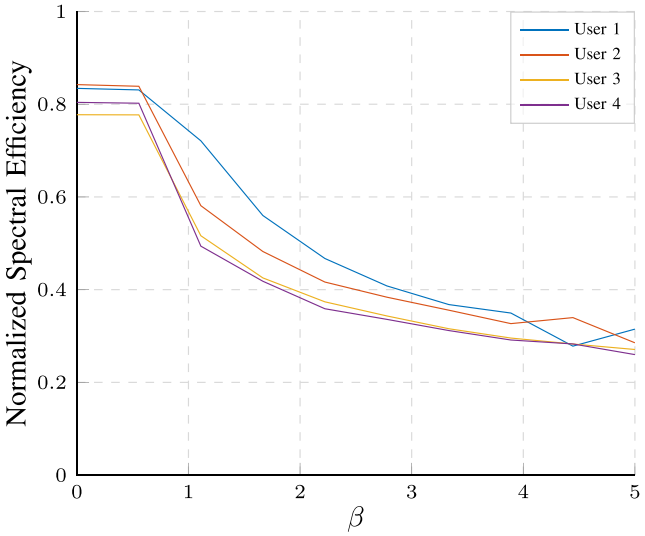

FIGURE 18. Normalized time-switched data rates w.r.t. β for $N_T = 10$ and $N = 4$. All elements in $\hat{\mu}_p$ are set to 1 and all elements in $\hat{\mu}_d$ are set to 10.

through the power allocation and then through the time-switching ratios. Fig. 16 shows that time-switching ratios are initially 1 for $\beta = 0$ due to data rate prioritization and decrease to 0.5 as fairness increases. Figs. 17 and 19 demonstrate that normalized Utopia data rates decrease while harvested powers increase with rising β, saturating at roughly $\beta = 2$. Finally, Figs. 18 and 20 reveal continuous increases in fairness as normalized time-switched data rates decrease and harvested powers increase to similar values as β increases up to 5. These results highlight the progressive impact of β on achieving equitable resource allocation.

Fairness may be measured through Jain's fairness index [51]. There are $2N$ objectives, so the index ranges from $\frac{1}{2N}$ (worst-case) to 1 (best-case), where 1 means that all users have the same allocation. The level of fairness between different user objectives for $N = 2$ and $N = 4$ w.r.t. the fairness parameter β is illustrated in Fig. 15. As expected, fairness increases as β increases from 0 to 5 for both the Utopia point and the time-switched point. Utopia point fairness appears to saturate earlier than time-switched point fairness, indicating that increasing fairness is first achieved through the power allocation and then by adjusting the time-switching ratio.

Fig. 16 illustrates the time-switching ratio as a function of the fairness parameter. For $\beta = 0$, the time-switching ratios are set to 1 due to weights favoring data rate over harvested power. As the fairness parameter increases, the time-switching ratio decreases to allow for more harvested power and increasing fairness. Interestingly, although individual user time-switching ratios diverge somewhat, they appear to converge to 0.5 with increasing fairness, which is ostensibly a fair value since it allocates half the time to decoding information and half the time to harvesting power. The time-switching ratios begin to diverge between $\beta = 1$ and $\beta = 2$ for user 1 and user 2, which is also where fairness for the Utopia point begins to saturate.

The effect of the fairness parameter on the individual objectives is illustrated for the normalized Utopia data rates in Fig. 17 and for the normalized Utopia powers in Fig. 19 as well as for the normalized time-switched data rates in Fig. 18 and for the normalized time-switched harvested powers in Fig. 20. Notice that the divergent time-switching ratios for user 1 and user 2 counteracts inequality between the respective power allocations for the utopia point. For example, user 1 has the highest Utopia data rate but has the lowest time-switching ratio. Likewise, user 2 has the highest Utopia power, but has the highest time-switching ratio. Lastly, although the plots have a generally smooth trend they also have one point at $\beta = 4.5$ that deviates from the

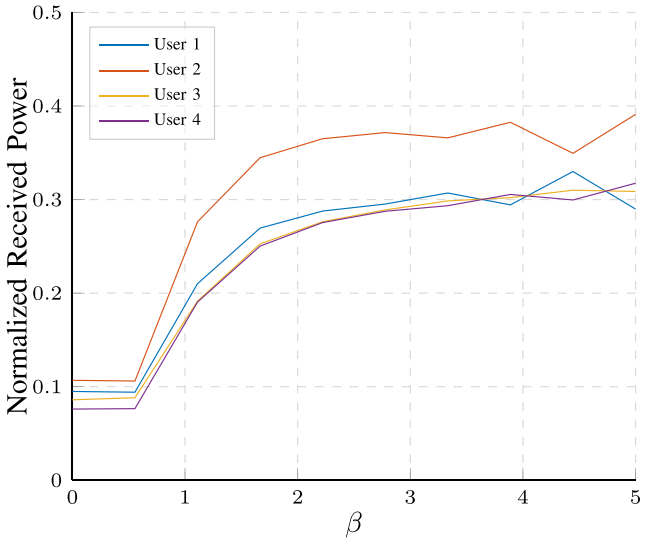

FIGURE 19. Normalized utopia power w.r.t. β for $N_T = 10$ and $N = 4$. All elements in $\hat{\mu}_p$ are set to 1 and all elements in $\hat{\mu}_d$ are set to 10.

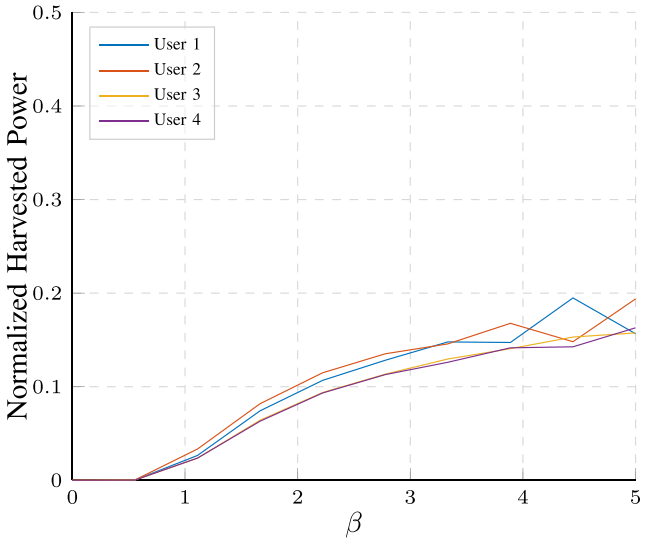

FIGURE 20. Normalized time-switched power w.r.t. β for $N_T = 10$ and $N = 4$. All elements in $\hat{\mu}_p$ are set to 1 and all elements in $\hat{\mu}_d$ are set to 10.

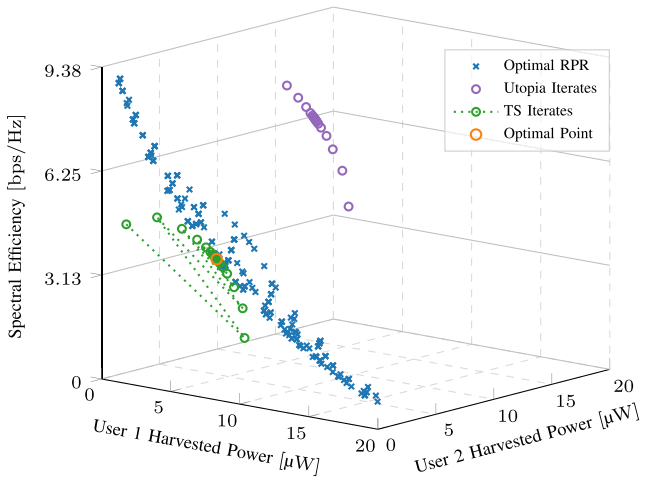

FIGURE 21. An example of the convergence of Algorithm 4 for $N_T = 10$, $N = 2$ users with arbitrary weights $\{\hat{\mu}_{p_n}, \hat{\mu}_{d_n}\}_{\forall n} = 1$, $\beta = 2$, and $\nu = 1$. The time-switched iterates (i.e., TS Iterates) produced by Algorithm 4 converge to a point on the Pareto edge of the Optimal RPR..

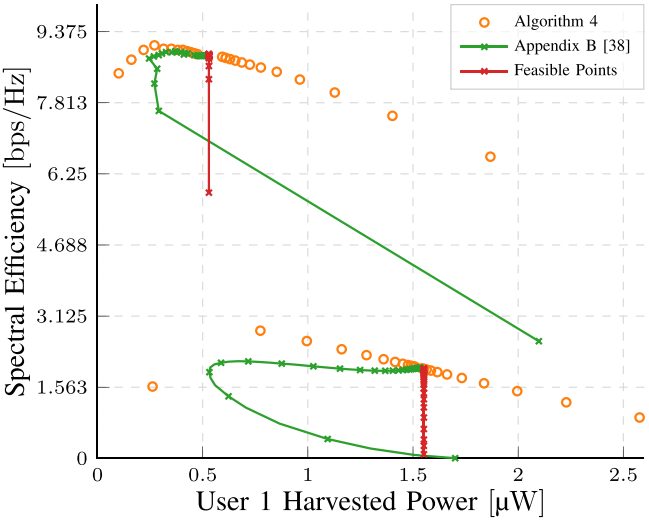

FIGURE 22. Iterates from Algorithm 4 with $\beta = 2$, $\nu = 1$, and $N = 2$ are shown here for two constraints ((0.529, 0.8565) and (1.551, 14.302) μW) based on the weights found in Appendix B in [42]. Algorithm 4 achieves the same spectral efficiency as [42, Appendix B] at the point that each constraint is met.

trend slightly. This is due to the convergence tolerance used; if the tolerances were tighter then the deviation would not exist. The tolerance was not increased to keep the simulation time reasonable.

C. COMPARISON WITH PRIOR WORK [7]

This subsection presents simulation results that confirm the consistency of the proposed algorithms with prior work and demonstrates Proposition 4. Proposition 4 simplifies the iterative process by setting $\nu = 1$ in (62) when $\beta = 2$, while still ensuring convergence of the time-switched iterates to the optimal value. Fig. 21 illustrates the convergence of Algorithm 4 when $\beta = 2$ and $\nu = 1$ to the optimal solution on the Pareto edge of the Optimal RPR, which was found using [7], [26] over a grid of power harvesting constraints. Additionally, Fig. 22 confirms that Algorithm 4 converges to the same optimal solution as [7] combined with the direction oracle. These results validate the proposed algorithms' effectiveness and alignment with established solutions.

Proposition 4 showed that when $\beta = 2$ and $\nu = 1$ the objective value for each iterate is the same. This enables simplifying the iteration by always setting $\nu = 1$ in (62). Fig. 21 demonstrates the time-switched iterates as the time-switching ratio converges to the optimal value for $\{\hat{\mu}_{p_n}, \hat{\mu}_{d_n}\}_{\forall n} = 1$ for $\beta = 2$ and $\nu = 1$ with Algorithm 4. At the optimal value, the time-switched point lies on the Pareto edge of the Optimal RPR. The Optimal RPR was created using by using the original algorithm in [7] to solve

for individual harvested power constraints within a grid of harvested powers.

To further illustrate, Algorithm 4 is used to optimize the time-switching ratio for the weights achieved in [42, Appendix B] for selected harvesting constraints shown in Fig. 22. [42, Appendix B] utilizes the original algorithm in [7] to consider the case where power harvesting constraints are specified and the optimal time-switching ratios are solved using the direction oracle. The optimization in Appendix B in [42] results in a set of weights $\{\lambda_n, \omega_n\}_{\forall n}$, optimal time-switching ratios $\boldsymbol{\alpha}^{\text{opt}}$, and the optimal time-switched point $\{\hat{r}_{p_n}, \hat{r}_{d_n}\}_{\forall n}$, which are associated with a Utopia point $\{r_{p_n}, r_{d_n}\}_{\forall n}$ and non-time-switched weights $\{w_{p_n}, w_{d_n}\}_{\forall n}$. Note that for user n, ω_n is a predefined weight for the data rate and λ_n is the Lagrange multiplier associated with the harvested power constraint. Solving for the non-time-switched weights and equating the result to (58) enables solving for the α-fair time-switched weights $\{\hat{\mu}_{p_n}, \hat{\mu}_{d_n}\}_{\forall n}$ given by

$$\left\{\hat{\mu}_{p_n} = \lambda_n \left(\hat{r}_{p_n}\right)^{\beta}, \hat{\mu}_{d_n} = \omega_n \left(\hat{r}_{d_n}\right)^{\beta}\right\}_{\forall n}. \tag{81}$$

These weights should result in the same solution. The initial time-switching ratios were all set to values that would better illustrate the progression of the iterates, rather than values that might converge more quickly, which can be seen converging in Fig. 22 to the same solutions found in [42]. The optimal points in Fig. 22 are where the red, green, and orange traces intersect.

VIII. PRACTICAL CONCERNS

A. IMPERFECT OR DELAYED CSI

This paper assumes perfect CSI at the transmitter, which is a standard simplification in initial algorithm design and performance benchmarking. This assumption isolates the impact of the proposed resource allocation scheme from that of channel uncertainty. In practice, acquiring high-accuracy CSI incurs significant overhead, either in the form of large feedback bandwidth or dense pilot tones, which is not always practical. As a result, CSI is often imperfect due to limited feedback, quantization errors, channel estimation inaccuracies, and feedback delays.

Under imperfect or delayed CSI, the performance of the proposed allocation scheme is expected to degrade. For instance, beamforming vectors computed using outdated or inaccurate CSI may be misaligned with the actual channel, reducing the received power and degrading the SINR. This affects both information decoding and power harvesting. Beamforming relies on accurate CSI to steer signal energy toward the intended user and to suppress interference toward others. When CSI is imperfect, the direction of the beam may not align with the actual channel, reducing array gain, lowering the SINR at the receiver, and degrading link quality. This also reduces the amount of harvestable power. The MMSE precoder employed in this paper is designed to optimally balance power transfer and interference suppression. However, under imperfect CSI, its interference mitigation capability is compromised, potentially leading to increased interference and reduced data rates. Consequently, the system may suffer losses in spectral efficiency, energy efficiency, and user fairness.

There are several mitigation strategies that can be employed such as optimizing performance under bounded CSI errors, utilizing stochastic formulations to model CSI uncertainty, or optimizing based on the correlation between the estimated channel and actual channel. Incorporating these techniques would allow the resource allocation to maintain performance even with imperfect CSI. Extending the proposed framework to handle CSI uncertainty is an important direction for future work. This could involve developing robust precoding and time-switching strategies that tolerate realistic CSI impairments, or adaptive schemes that exploit channel statistics and feedback dynamics.

B. TIME-SWITCHING PRACTICALITIES

While time-switching is conceptually low-complexity, its practical implementation involves several trade-offs in cost, timing, and granularity:

- *Implementation Cost:* Time-switching can be practically implemented using existing commercial off-the-shelf (COTS) OFDM transceivers, fast microcontrollers, and a high-speed RF switch–all at a reasonable cost. For instance, the ADG918/9 RF switch [14] is available for 4.25 euros or less [52], and the SiWG917, which integrates a WiFi transceiver and a 32-bit microcontroller [53], can be sourced for under 6 euros [54]. This low implementation cost is a key advantage of time-switching.
- *Granularity Limits:* In OFDM, each QAM symbol is assigned to a subcarrier and spread across multiple time-domain samples by the IFFT. As a result, an entire OFDM symbol conveys a single, meaningful QAM symbol per subcarrier. Therefore, an OFDM symbol cannot simultaneously carry information (via meaningful QAM symbols) and serve as a dummy symbol for power harvesting. This makes switching between information decoding and power harvesting within a single OFDM symbol infeasible.
  Although time-switching is typically modeled with arbitrary resolution, the structure of the OFDM symbol imposes a granularity constraint: switching can only occur at the level of full OFDM symbols, including the cyclic prefix. This limits how finely energy and information periods can be divided. While this coarse granularity may reduce optimality, it is often negligible in practice. OFDM frames typically span hundreds of microseconds, whereas switching at the resolution of a single OFDM symbol introduces minimal overhead. For instance, in IEEE 802.11a, the duration of one OFDM symbol (including the cyclic prefix) is $T_{\text{Symbol}} = 1.25 \cdot \frac{K}{f_s} = 1.25 \cdot \frac{64}{20\text{MHz}} = 4\mu\text{s}$ [55]. If a data transmission

lasts up to 1ms, then the switching granularity of 4, µs constitutes only 0.4%, which is relatively insignificant.

- *Timing and Control:* Real-time time-switching control must be based on information extracted early in the data frame. Since decoding can be designed to precede power harvesting, the time-switching ratio can be determined from length fields embedded in the initial OFDM symbols, or potentially through pilot tones. This approach requires a minimum amount of information decoding, meaning a frame cannot be used exclusively for power harvesting. Ideally, a SWIPT receiver would integrate time-switching control to maximize the range of feasible time-switching ratios. However, an external microcontroller and RF switch can also manage this control, albeit with the trade-off of increasing the minimum decoding requirement due to the latency involved in transferring received OFDM symbols to the microcontroller.

  Fine-grained timing is essential to accurately transition between decoding and harvesting. Once the time-switching ratio is determined for a given frame, timer-based interrupts can be used to trigger the transition to harvesting. COTS microcontrollers and RF switches can toggle states via GPIO within 10 ns [14], [53], which is negligible compared to the OFDM symbol period. After switching, the device can remain in harvesting mode until the next frame or beacon interval.
- *Power and Latency Overhead:* The RF switch introduces negligible power overhead–for instance, the ADG918/9 [14] draws less than 1 µA. In contrast, the radio is typically among the most power-hungry components in a wireless device. For example, the SiWG917 has a typical listening current of 16.5 mA. Time-switching, by encouraging radio duty cycling, offers the potential for significant energy savings. However, duty cycling introduces network-level complexity. Radio wake-up latency can range from 10 to 100 µs, which may be impractical for frequent switching. To address this, sleep-wake transitions should be minimized–e.g., occurring once per frame or over aggregated transmissions. Additionally, switching to harvesting mode requires buffering data until the next decoding interval. As a result, larger data volumes introduce a trade-off between communication latency and device energy longevity.

These considerations justify the practicality of time-switching in real-world OFDM systems while acknowledging trade-offs in timing precision and energy efficiency due to hardware constraints.

IX. CONCLUSION

In this paper, the results from both [7] and [26] were combined into an efficient near-optimal resource allocation method that jointly allocates power, designs precoding vectors, and chooses per-user time-switching ratios for a MU-MISO-BC SWIPT system employing OFDM to maximize a weighted sum of α-fair data rates and harvested powers. We considered a use case that incorporates fairness and does not support specific power harvesting constraints. The objective for the resource allocation problem is first generalized from a weighted sum of data rates to a weighted sum of data rates and harvested powers individually encapsulated in α-Fairness utility functions. Equations for the optimal time-switching ratios as a function of the fairness parameter and resource allocation are derived for the α-fair objective. Due to the time-switching ratios coupling the subcarriers, an AO is utilized to alternately optimize the precoding vectors, power allocation, and the time-switching ratios. To support this, the resource allocation problem presented in [7] is reformulated as a weighted sum of data rates and harvested powers, which is then used to iteratively solve the resource allocation problem considered here but for fixed time-switching ratios. The time-switching ratios are then adjusted in the ascent direction based on a mapping derived from the mapping presented in [26]. The resulting formulation led to new insights into the relationship between the time-switching ratio, the system weights, and the fairness parameter, which resulted in a near-optimal relative resource allocation method that incorporates varying levels of fairness.

A direction for future work involves addressing the practical limitations of implementing time-switching and beamforming in real-world SWIPT systems. While OFDM's cyclic prefix provides a robust timing structure that facilitates symbol-level synchronization, the precision of time-switching circuits at the receiver remains a concern due to hardware-induced delays, switching transients, and potential misalignment under noisy or time-varying conditions. Developing adaptive or tolerant switching schemes that maintain performance despite such imperfections would improve implementation feasibility. Similarly, the joint precoding and power allocation strategy presented in this work assumes ideal, unconstrained beamforming capabilities at the transmitter. In practice, hardware impairments–such as a restricted number of RF chains and nonlinearities in power amplifiers–can degrade the quality of the beamforming vectors. Future research should consider incorporating these constraints into the optimization framework, exploring hardware-aware beamforming designs or robust precoding methods that preserve fairness and SWIPT performance under practical limitations like imperfect CSI.

REFERENCES

[1] L. R. Varshney, "Transporting information and energy simultaneously," in *Proc. IEEE Int. Symp. Inf. Theory*, 2008, pp. 1612–1616.
[2] P. Grover and A. Sahai, "Shannon meets Tesla: Wireless information and power transfer," in *Proc. IEEE Int. Symp. Inf. Theory*, 2010, pp. 2363–2367.
[3] R. Zhang and C. K. Ho, "MIMO broadcasting for simultaneous wireless information and power transfer," *IEEE Trans. Wireless Commun.*, vol. 12, no. 5, pp. 1989–2001, May 2013.
[4] X. Lu, P. Wang, D. Niyato, D. I. Kim, and Z. Han, "Wireless networks with RF energy harvesting: A contemporary survey," *IEEE Commun. Surveys Tuts.*, vol. 17, no. 2, pp. 757–789, 2nd Quart., 2015.

[5] S. Hayashi and Z.-Q. Luo, "Dynamic spectrum management: When is FDMA sum-rate optimal?" in *Proc. IEEE Int. Conf. Acoust., Speech Signal Process. (ICASSP)*, 2007, pp. 609–612.

[6] E. Björnson, M. Bengtsson, and B. Ottersten, "Optimal multiuser transmit beamforming: A difficult problem with a simple solution structure [lecture notes]," *IEEE Signal Process. Mag.*, vol. 31, no. 4, pp. 142–148, Jul. 2014.

[7] R. P. Ketcham, J. Verdyck, and M. Moonen, "Joint beamforming and power allocation for multiuser MISO broadcast channel SWIPT employing OFDM," *IEEE Access*, vol. 9, pp. 165154–165172, 2021.

[8] W. Yu and R. Lui, "Dual methods for nonconvex spectrum optimization of multicarrier systems," *IEEE Trans. Commun.*, vol. 54, no. 7, pp. 1310–1322, Jul. 2006.

[9] Z.-Q. Luo and S. Zhang, "Dynamic spectrum management: Complexity and duality," *IEEE J. Sel. Topics Signal Process.*, vol. 2, no. 1, pp. 57–73, Feb. 2008.

[10] T. D. P. Perera, D. N. K. Jayakody, S. K. Sharma, S. Chatzinotas, and J. Li, "Simultaneous wireless information and power transfer (SWIPT): Recent advances and future challenges," *IEEE IEEE Commun. Surveys Tuts.*, vol. 20, no. 1, pp. 264–302, 1st Quart., 2018.

[11] M. Mohammadi, L.-N. Tran, Z. Mobini, H. Q. Ngo, and M. Matthaiou, "Cell-free massive MIMO and SWIPT: Access point operation mode selection and power control," in *Proc. IEEE Glob. Commun. Conf. (GLOBECOM)*, 2023, pp. 661–666.

[12] M. Amiri et al., "Stacked intelligent metasurface for simultaneous wireless information and power transfer," in *Proc. IEEE Int. Conf. Commun. (ICC)*, 2025, pp. 1–6.

[13] J. Saraswat and P. P. Bhattacharya, "Effect of duty cycle on energy consumption in wireless sensor networks," *Int. J. Comput. Netw. Commun.*, vol. 5, no. 1, pp. 125–140, Jan. 2013.

[14] "ADG918/ADG919 wideband 4 GHz, 43 dB isolation at 1 GHz, CMOS 1.65 V to 2.75 V, 2:1 Mux/SPDT," Data Sheet, AnalogDevices, Wilmington, MA, USA. Accessed: May 27, 2025. [Online]. Available: https://www.analog.com/media/en/technical-documentation/data-sheets/ADG918_919.pdf

[15] S. Ilyas, N. Shoaib, S. Nikolaou, and H. M. Cheema, "A wideband tunable power divider for SWIPT systems," *IEEE Access*, vol. 8, pp. 30675–30681, 2020.

[16] B. Wu, Z. Sun, X. Wang, Z. Ma, and C.-P. Chen, "A reconfigurable Wilkinson power divider with flexible tuning range configuration," *IEEE Trans. Circuits Syst. II, Exp. Briefs*, vol. 67, no. 7, pp. 1219–1223, Jul. 2020.

[17] T. M. Hoang, B. C. Nguyen, N. N. Thang, M. Tran, and P. T. Tran, "Performance and optimal analysis of time-switching energy harvesting protocol for MIMO full-duplex decode-and-forward wireless relay networks with various transmitter and receiver diversity techniques," *J. Frankl. Inst.*, vol. 357, no. 17, pp. 13205–13230, Nov. 2020.

[18] M. Mohammadi, B. K. Chalise, H. A. Suraweera, C. Zhong, G. Zheng, and I. Krikidis, "Throughput analysis and optimization of wireless-powered multiple antenna full-duplex relay systems," *IEEE Trans. Commun.*, vol. 64, no. 4, pp. 1769–1785, Apr. 2016.

[19] C. Zhong, H. A. Suraweera, G. Zheng, I. Krikidis, and Z. Zhang, "Wireless information and power transfer with full duplex relaying," *IEEE Trans. Commun.*, vol. 62, no. 10, pp. 3447–3461, Oct. 2014.

[20] C. Zhong, X. Chen, Z. Zhang, and G. K. Karagiannidis, "Wireless-powered communications: Performance analysis and optimization," *IEEE Trans. Commun.*, vol. 63, no. 12, pp. 5178–5190, Dec. 2015.

[21] B. K. Chalise, H. A. Suraweera, and G. Zheng, "Throughput maximization for full-duplex energy harvesting MIMO communications," in *Proc. IEEE 17th Int. Workshop Signal Process. Adv. Wireless Commun. (SPAWC)*, 2016, pp. 1–5.

[22] L. Ma, Y. Wang, and Y. Xu, "Sum rate optimization for SWIPT system based on zero-forcing beamforming and time switching," in *Proc. 13th Int. Wireless Commun. Mobile Comput. Conf. (IWCMC)*, 2017, pp. 351–356.

[23] X. Zhou, R. Zhang, and C. K. Ho, "Wireless information and power transfer in multiuser OFDM systems," *IEEE Trans. Wireless Commun.*, vol. 13, no. 4, pp. 2282–2294, Apr. 2014.

[24] J. Tang, D. K. C. So, N. Zhao, A. Shojaeifard, and K.-K. Wong, "Energy efficiency optimization with SWIPT in MIMO broadcast channels for Internet of Things," *IEEE Internet Things J.*, vol. 5, no. 4, pp. 2605–2619, Aug. 2018.

[25] S. Kang, H. Lee, S. Hwang, and I. Lee, "Time switching protocol for multi-antenna SWIPT systems," in *Proc. IEEE Wireless Commun. Netw. Conf. (WCNC)*, 2020, pp. 1–6.

[26] R. Ketcham, J. Verdyck, and M. Moonen, "Optimal time-switching for simultaneous wireless information and power transfer," in *Proc. IEEE Int. Mediterr. Conf. Commun. Netw. (MeditCom)*, 2022, pp. 304–309.

[27] J. Mo and J. Walrand, "Fair end-to-end window-based congestion control," *IEEE/ACM Trans. Netw.*, vol. 8, no. 5, pp. 556–567, Oct. 2000.

[28] J.-M. Kang, I.-M. Kim, and D. I. Kim, "Joint Tx power allocation and Rx power splitting for SWIPT system with multiple nonlinear energy harvesting circuits," *IEEE Wireless Commun. Lett.*, vol. 8, no. 1, pp. 53–56, Feb. 2019.

[29] G. Ma, J. Xu, Y. Zeng, and M. R. V. Moghadam, "A generic receiver architecture for MIMO wireless power transfer with nonlinear energy harvesting," *IEEE Signal Process. Lett.*, vol. 26, no. 2, pp. 312–316, Feb. 2019.

[30] J. Brehmer, *Utility Maximization in Nonconvex Wireless Systems* (Foundations in Signal Processing, Communications and Networking), vol. 5. Berlin, Germany: Springer, 2012.

[31] A. Messac, C. Puemi-Sukam, and E. Melachrinoudis, "Aggregate objective functions and Pareto frontiers: Required relationships and practical implications," *Optim. Eng.*, vol. 1, pp. 171–188, Jul. 2000.

[32] J. Verdyck and M. Moonen, "Dynamic spectrum management in digital subscriber line networks with unequal error protection requirements," *IEEE Access*, vol. 5, pp. 18107–18120, 2017.

[33] J. Verdyck, W. Lanneer, P. Tsiaflakis, W. Coomans, P. Patrinos, and M. Moonen, "Optimal dynamic spectrum management algorithms for multi-user full-duplex DSL," *IEEE Access*, vol. 7, pp. 106600–106616, 2019.

[34] V. L. Nir, M. Moonen, J. Verlinden, and M. Guenach, "Optimal power allocation for downstream xDSL with per-modem total power constraints: Broadcast Channel Optimal Spectrum Balancing (BC-OSB)," *IEEE Trans. Signal Process.*, vol. 57, no. 2, pp. 690–697, Feb. 2009.

[35] W. Yu and T. Lan, "Transmitter optimization for the multi-antenna downlink with per-antenna power constraints," *IEEE Trans. Signal Process.*, vol. 55, no. 6, pp. 2646–2660, Jun. 2007.

[36] R. Hunger, M. Joham, and W. Utschick, "On the MSE-duality of the broadcast channel and the multiple access channel," *IEEE Trans. Signal Process.*, vol. 57, no. 2, pp. 698–713, Feb. 2009.

[37] D. Tse and P. Viswanath, *Fundamentals of Wireless Communication*. Cambridge, U.K.: Cambridge Univ. Press, 2005.

[38] E. Björnson, J. Hoydis, and L. Sanguinetti, "Massive MIMO networks: Spectral, energy, and hardware efficiency," *Found. Trends® Signal Process.*, vol. 11, nos. 3–4, pp. 154–655, 2017.

[39] M. Razaviyayn, M. Hong, and Z.-Q. Luo, "A unified convergence analysis of block successive minimization methods for nonsmooth optimization," *SIAM J. Optim.*, vol. 23, no. 2, pp. 1126–1153, Jan. 2013.

[40] G. Scutari, F. Facchinei, P. Song, D. P. Palomar, and J.-S. Pang, "Decomposition by partial linearization: Parallel optimization of multi-agent systems," *IEEE Trans. Signal Process.*, vol. 62, no. 3, pp. 641–656, Feb. 2014.

[41] M. Jaggi, "Revisiting Frank-Wolfe: Projection-free sparse convex optimization," in *Proc. 30th Int. Conf. Int. Conf. Mach. Learn.*, 2013, pp. 427–435.

[42] R. Ketcham, "Optimal resource allocation for simultaneous wireless information and power transfer in multiuser MISO-OFDM systems," Ph.D. dissertation, Dept. Electr. Eng., KU Leuven, Leuven, Belgium, Sep. 2024.

[43] K. B. Petersen and M. S. Pedersen, *The Matrix Cookbook*, Tech. Univ. Denmark, Lyngby, Denmark, Nov. 2012.

[44] M. Hong, M. Razaviyayn, Z.-Q. Luo, and J.-S. Pang, "A unified algorithmic framework for block-structured optimization involving big data: With applications in machine learning and signal processing," *IEEE Signal Process. Mag.*, vol. 33, no. 1, pp. 57–77, Jan. 2016.

[45] K. Sikorski, "Bisection is optimal," *Numerische Mathematik*, vol. 40, no. 1, pp. 111–117, Feb. 1982.

[46] G. Garrigos and R. M. Gower, "Handbook of convergence theorems for (stochastic) gradient methods," 2024, *arXiv:2301.11235*.

[47] H. Hijazi, L. Ros, and G. Jourdain, "OFDM channel parameters estimation used for ICI reduction in time-varying multipath channels," in *Proc. 13th Eur. Wireless Conf. (EW)*, 2007, p. 6.

[48] A. Goldsmith, *Wireless Communications*. Cambridge, U.K.: Cambridge Univ. Press, 2005.

[49] (MathWorks, Natick, MA, USA). *Filter Input Signal Through MIMO Multipath Fading Channel*. (2018). [Online]. Available: https://nl.mathworks.com/help/comm/ref/comm.mimochannel-system-object.html

[50] R. Jain, *Channel Models a Tutorial V1.0*, Washington Univ., St. Louis, MO, USA, 2007.

[51] R. K. Jain, D.-M. W. Chiu, and W. R. Hawe, "A quantitative measure of fairness and discrimination for resource allocation in shared computer systems," East. Res. Lab., Digit. Equip. Corp., Hudson, MA, USA, Rep. TR-301, Sep. 1984.

[52] "Analog devices | mouser Belgium," Data Sheet ADG918BCPZ-500RL7, Mouser Electron. Co., Mansfield, TX, USA. Accessed: May 27, 2025. [Online]. Available: https://www.mouser.be/ProductDetail/Analog-Devices/ADG918BCPZ-500RL7?qs=BpaRKvA4VqFQVutXSJ%2%%3D

[53] *SiWG917 SoC Single Chip Wi-Fi and Bluetooth LE Wireless Secure MCU Solutions*, Silicon Labs, Austin, TX, USA, Dec. 2024.

[54] "Silicon labs | mouser," Data Sheet SiWT917M100XGTBA, Mouser Electron. Co., Mansfield, TX, USA. Accessed: May 27, 2025. [Online]. Available: https://www.mouser.be/ProductDetail/Silicon-Labs/SiWT917M100XGTBA?qs=IK%2F947nfChUplRANvd%%3D

[55] *IEEE Standard for Information Technology—Telecommunications and Information Exchange Between Systems Local and Metropolitan Area Networks—Specific Requirements—Part 11: Wireless LAN Medium Access Control (MAC) and Physical Layer (PHY) Specifications*, IEEE Standard 802.11-2016 (Revision of IEEE Std 802.11-2012), Dec. 2016.